

Article citation info:

Zhang H, Song L, Adaptive subregion-based active Kriging for collaborative multi-failure reliability assessment, *Eksploracja i Niezawodność – Maintenance and Reliability* 2026; 28(3) <http://10.17531/ein/216133>

Adaptive subregion-based active Kriging for collaborative multi-failure reliability assessment

Indexed by:



Hong Zhang^a, Lu-Kai Song^{b,*}

^a School of Mechanical and Electrical Engineering, Suqian University, Jiangsu, China

^b School of Mechanical Engineering, University Science and Technology Beijing, Beijing, China

Highlights

- Proposes adaptive subregion-based active Kriging (AS-AK) method.
- Enhances efficiency and accuracy in multi-failure reliability assessment.
- Integrates active learning with adaptive subregion decomposition.
- Validated on four benchmarks and aeroengine rigid-flexible system.
- Outperforms traditional methods in accuracy and computational cost.

Abstract

This paper proposes an adaptive subregion-based active Kriging (AS-AK) surrogate modeling approach. Firstly, an adaptive subregion decomposition strategy is developed to partition the candidate sample space into multiple concentric subregions, significantly enhancing the efficiency and accuracy of sampling. Subsequently, an active Kriging surrogate model is constructed, where the surrogate model is sequentially updated by iteratively selecting critical samples within each subregion to precisely approximate the highly nonlinear limit state function. Moreover, a collaborative multi-output surrogate modeling framework is further established to systematically handle correlations among multiple failure modes. Four benchmark numerical examples and an engineering application involving an aeroengine rigid-flexible coupling system illustrate that the proposed AS-AK method significantly outperforms existing reliability methods in both computational efficiency and accuracy.

Keywords

system reliability, multi-failure, Kriging model, active learning, sampling

This is an open access article under the CC BY license (<https://creativecommons.org/licenses/by/4.0/>)

1. Introduction

The reliability of aeroengine rigid-flexible coupling systems directly influences overall engine performance by maintaining stable operation through precise adjustments of stator blade angles. However, due to the complexity of their internal structures and harsh operating conditions [1-3], these systems often experience deviations between the actual rotation angles and designed values of stator blades, leading to insufficient motion accuracy. Over extended periods, such deviations significantly impact the reliability and safety of aeroengines, making motion accuracy failures a predominant concern.

Furthermore, the uncertainties inherent in material properties [4-5], loading conditions [6-7], and dimensional tolerances [8-9] contribute to high nonlinearity and complex correlations among multiple failure modes. Traditional reliability methods typically face considerable challenges in accurately modeling these nonlinear and correlated failure characteristics [10-12]. Therefore, there is an urgent need for efficient and precise reliability assessment methods that adequately consider uncertainties and correlations among multiple failure modes.

Currently, reliability analysis methods mainly comprise

(*) Corresponding author.

E-mail addresses:

H. Zhang, (ORCID: 0000-0002-9784-5370) zhanghong_2009@126.com, L. Song (ORCID: 0009-0004-3053-6858) slk@ustb.edu.cn

approximate analytical methods [13-15], numerical simulation approaches [16-18], and surrogate modeling techniques [19-21]. Among these, surrogate modeling has gained popularity due to its effectiveness in approximating the true limit state function (LSF) with mathematical surrogate models, particularly for simple structural reliability problems [22-24]. Active learning surrogate modeling techniques, which iteratively select critical samples based on specific learning criteria, have emerged as powerful approaches for significantly improving surrogate modeling accuracy [25-28]. Notably, the adaptive Kriging (AK) method, integrating active learning strategies with the Kriging surrogate model, has proven particularly advantageous in handling reliability problems characterized by small failure probability [29-31]. Meanwhile, the active learning Kriging method is also widely applied in reliability-based design optimization for complex structures. Meng et al. [32-34] proposed AK-based reliability analysis methods and developed them into uncertainty design optimization.

However, traditional AK-based methods combined with Monte Carlo simulation (AK-MCS) often suffer from low computational efficiency, primarily due to the excessively large number of candidate samples required for accurate modeling of small-probability events [35-36]. To mitigate this computational burden while preserving accuracy, researchers have introduced various variance-reduction techniques, such as Line Sampling (LS) [37-39], Directional Sampling (DS) [40-42], Subset Simulation (SS) [43-45], and Importance Sampling (IS) [46-48], into AK-based reliability analysis framework. For instance, Tong et al. [49] enhanced active learning reliability methods by combining AK models with subset simulation-based importance sampling. Echard et al. [50] presented a practical AK-IS framework for efficiently assessing small failure probability. Similarly, Wang et al. [51] proposed integrating multi-loop importance sampling with adaptive Kriging to improve computational efficiency. Yang et al. [52] developed a concentric ring approximation strategy to estimate rare-event probability, and Yun et al. [53] combined adaptive radial importance sampling with AK for efficient failure boundary identification.

Despite these advancements, the existing AK-based methods have not fully addressed the computational challenges posed by complex, nonlinear, multi-failure mode reliability

analyses. In response, this paper proposes an adaptive subregion-based active Kriging (AS-AK) surrogate modeling method. The core idea is to adaptively partition the candidate sample space into multiple concentric subregions, significantly reducing sampling redundancy and enhancing computational efficiency. Critical samples are actively selected within each subregion to progressively update and refine the surrogate model, precisely capturing the nonlinear limit state functions. Furthermore, a collaborative multi-failure reliability analysis framework is established by integrating multiple AS-AK surrogate models, systematically accounting for correlations among different failure modes. The effectiveness and advantages of the proposed AS-AK method are demonstrated through four numerical benchmark cases and an engineering application involving an aeroengine rigid-flexible coupling system, validating its superior performance in computational efficiency and accuracy compared with state-of-the-art methods. Compared with the existing methods, the advantages of the proposed method mainly include three aspects: (1) adaptive subregion decomposition strategy reduces the number of candidate samples in the process of updating the surrogate model, thus accelerating the identification of critical training points and enhancing computational efficiency. (2) the linkage sampling technique ensures the accuracy of the multi-failure reliability model by considering the correlations among different failure modes. (3) collaborative multi-failure reliability analysis framework reduces the complexity and computational cost in multi-failure system reliability assessment, and improves the computational efficiency of aeroengine rigid-flexible coupling system.

The rest of this paper is organized as follows. Section 2 details the theoretical formulation of the AS-AK method, including the active Kriging model and adaptive subregion decomposition strategy. Section 3 describes the collaborative multi-failure reliability framework based on AS-AK surrogate model. Section 4 presents numerical examples to illustrate the method's performance, followed by an engineering case study on an aeroengine rigid-flexible coupling system in Section 5. Finally, conclusions and insights are summarized in Section 6.

2. Theoretical formulations of AS-AK

To efficiently evaluate the reliability of systems with multiple

correlated failure modes, high nonlinearity, and small failure probability, this section proposes the detailed theoretical formulation of the adaptive subregion-based active Kriging method. The AS-AK integrates two core innovations: an adaptive subregion decomposition strategy to optimize the sample distribution, and an active learning-based Kriging model to iteratively refine the surrogate model toward accurate approximations of complex limit state function.

2.1. Active Kriging model (AK)

Given an initial set of training samples $\mathbf{x} = [x_1, x_2, \dots, x_s]$ and their corresponding responses $y_0(\mathbf{x})$, the initial Kriging surrogate model can be mathematically expressed as follows [54]:

$$y_0(\mathbf{x}) = \mathbf{f}^T(\mathbf{x})\boldsymbol{\beta} + z(\mathbf{x}) \quad (1)$$

where $\mathbf{f}^T(\mathbf{x}) = [f_1(\mathbf{x}), f_2(\mathbf{x}), \dots, f_d(\mathbf{x})]$ indicates the vector of regression basis function; $\boldsymbol{\beta} = [\beta_1, \beta_2, \dots, \beta_d]$ the vector of the unknown regression coefficient; $z(\mathbf{x})$ the Gaussian random deviation with zero mean and variance σ^2 .

To efficiently select the most informative samples and enhance surrogate model accuracy, an active learning criterion named improved reliability-based expected improvement function (REIF2) [55] is adopted. Initially, a large-scale set of candidate samples $\{x_1, x_2, \dots, x_N\}$ is generated using Latin Hypercube Sampling. Then, the optimal candidate sample x_k is selected by maximizing the following REIF2 function [55]:

$$\begin{aligned} REIF2(\mathbf{x}) = & \mu_{\hat{y}} f_x(\mathbf{x}) \left[1 - 2\phi\left(\frac{\mu_{\hat{y}}}{\sigma_{\hat{y}}}\right) \right] \\ & + \sigma_{\hat{y}} \left[\alpha - \sqrt{\frac{2}{\pi}} \exp\left(-\frac{1}{2}\left(\frac{\mu_{\hat{y}}}{\sigma_{\hat{y}}}\right)^2\right) \right] \end{aligned} \quad (2)$$

where $\mu_{\hat{y}}$ denotes the predicted mean function; $\sigma_{\hat{y}}$ the predicted standard deviation function; α the weight constant of the adjustment $\mu_{\hat{y}}$ and $\sigma_{\hat{y}}$; $f_x(\mathbf{x})$ the joint probability density function.

After identifying the most valuable sample $x_k = \text{argmax}\{REIF2(\mathbf{x})\}$, the training dataset is updated, and the surrogate model $y_k(\mathbf{x})$ is refined as follows

$$\begin{aligned} y_k(\mathbf{x}) & = \left\{ y_0(\mathbf{x}) | S_0 \xrightarrow{\text{Active learning REIF2 function}} y_k(\mathbf{x}) | S_k \right\} \quad (3) \\ & = \mathbf{f}^T(\mathbf{x})\boldsymbol{\beta} + z(\mathbf{x}) \end{aligned}$$

This active-learning iterative process progressively enhances the surrogate model accuracy near critical regions associated with small failure probability.

2.2. Adaptive subregion strategy (AS)

To efficiently identify critical samples and enhance the surrogate modeling accuracy near failure boundaries, an adaptive subregion strategy (AS) is developed. The key idea behind AS is to partition the original candidate sample space into multiple concentric and non-overlapping subregions, allowing a more targeted and efficient exploration of regions near the limit state function. The schematic illustration of this adaptive decomposition is depicted in **Fig. 1**.

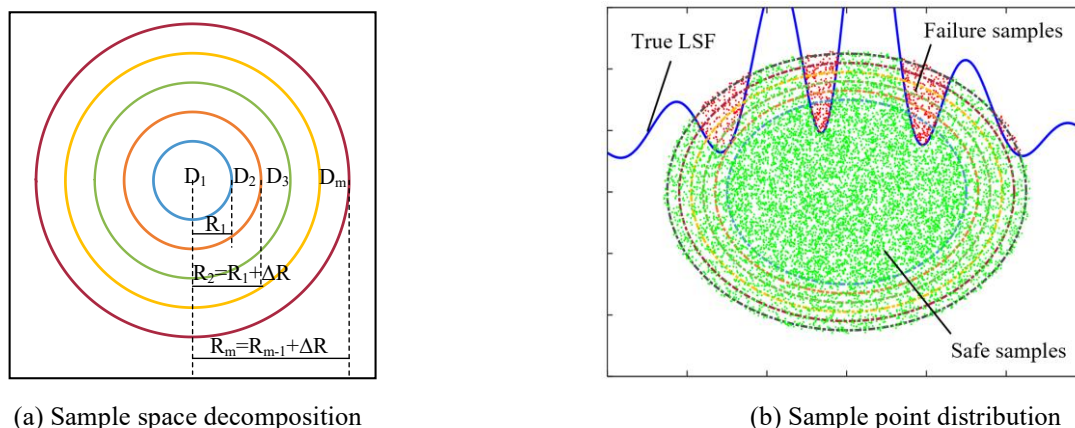


Fig. 1. Schematic diagram of the adaptive subregion strategy.

As shown in **Fig. 1**, in the standard normal space, the candidate sample space $D = R_N$ is adaptively decomposed into several concentric ring-shaped subregions D_i . Each subregion D_i is defined by its inner radius R_{i-1} and outer radius R_i , satisfying:

$$D = \bigcup_{i=1}^m D_i \quad (4)$$

$$D_i \cap D_j = \emptyset, i \neq j \quad (5)$$

$$D_i = \{x | R_{i-1} \leq \|x\|_2 < R_i, x \in D\} \quad (6)$$

where $R_0 = 0$ and the radius sequence R_i is adaptively determined by the sample distribution and convergence criteria.

To generate candidate samples within each subregion D_i , the following sampling formula is adopted:

$$X_{D_i} = \sqrt[d]{R_{i-1}^d + (R_i^d - R_{i-1}^d) \times \xi} \times \frac{x}{\|x\|_2} \quad (7)$$

where d denotes the dimensionality of the parameter space and ξ is a random number uniformly distributed between 0 and 1. By independently controlling the candidate sample size in each subregion, the proposed AS strategy effectively reduces redundant sampling, thereby significantly improving the modeling efficiency. After applying the adaptive subregion decomposition, the overall failure probability P_f can be expressed as

$$P_f = \int_{\cup_{i=1}^m D_i} I_F(x) f_x(x) dx = \sum_{i=1}^m \int_{D_i} I_F(x) f_x(x) dx \quad (8)$$

where x is the input random variables; $f_x(x)$ the joint probability density function (PDF) of x ; $I_F(x)$ is the indicator function of the failure domain, which can be expressed as

$$I_F(x) = \begin{cases} 1, & x \in F \\ 0, & \text{else} \end{cases} \quad (9)$$

where F representing the failure domain where the limit state function $g(x) \leq 0$.

Considering the advantages of importance sampling in enhancing sampling efficiency and accelerating convergence, the failure probability within each subregion can be further estimated [56] by:

$$P_f' = \int_{D_i} I_F(x) \frac{f_x(x)}{h(x)} dx \quad (10)$$

$$h(x) = \frac{I_F(x) f_x(x)}{P_f} \quad (11)$$

where $h(x)$ is the importance sampling probability density function. Typically, $h(x)$ is chosen according to the volume of the m -dimensional hypersphere, given by $V_m = (\pi^{m/2} R^m) / \Gamma(m/2 + 1)$, with $\Gamma(\cdot)$ representing the gamma function and R the radius of the sampling region. The adaptive subregion decomposition strategy combined with the importance sampling method ensures that more candidate samples surround the limit state function, which greatly reduces the search efficiency of the optimal training samples and improves the modeling accuracy of the surrogate model.

During the iterative process, the surrogate model convergence is monitored using the following convergence criterion $\varepsilon = \frac{|P_f^k - P_f^{k+1}|}{P_f^{k+1}} < \delta$. Once this criterion is satisfied,

further expansion of the sampling subregion is halted, and the surrogate model approximation meets the required accuracy. Note that with the continuous update of the Kriging model, when the failure probability of subregion does not meet the convergence requirement, the subregion will be further expanded, thereby ensuring that the real LSF can be effectively approximated.

2.3. Adaptive subregion strategy-based AK (AS-AK)

To systematically leverage the advantages of active learning for precise sample selection and adaptive subregion decomposition for efficient candidate sample management, an integrated adaptive subregion-based active Kriging surrogate modeling method is proposed. The flowchart of the proposed AS-AK method is presented in Fig. 2, with detailed procedural steps outlined as follows:

Step 1: Initial surrogate model construction. Initial training samples are generated using Latin hypercube sampling (LHS) [18], and the corresponding responses are computed by simulation or calling the real LSF. An initial Kriging surrogate model is established based on these samples.

Step 2: Adaptive subregion parameter initialization. Set the initial parameters of the adaptive subregion decomposition strategy, including the initial inner radius, the initial outer radius, and the candidate sample size allocated within each subregion.

Step 3: Active surrogate model updating. Candidate sample points are generated within the current subregion. The surrogate model is iteratively updated by selecting the most informative sample from this candidate set, guided by the REIF2 active learning criterion. These critical samples are subsequently incorporated into the existing training dataset to refine the surrogate model approximation.

Step 4: Failure probability estimation and convergence checking. Using the updated surrogate model and the importance sampling technique, estimate the current failure probability. Evaluate the convergence criterion $\varepsilon = \frac{|P_f^k - P_f^{k+1}|}{P_f^{k+1}} < \delta$ based on the estimated failure probability. If convergence is achieved (i.e., the ε falls below a predefined threshold), proceed to Step 5. Otherwise, expand the sampling region adaptively outward, return to Step 3, and repeat the sampling and updating process. Importantly, previously evaluated samples are fully retained to ensure computational efficiency and avoid redundant

simulations.

Step 5: Output final results and terminate algorithm.

Once the convergence criterion is satisfied, output the estimated

failure probability as the final reliability assessment result, and terminate the AS-AK algorithm.

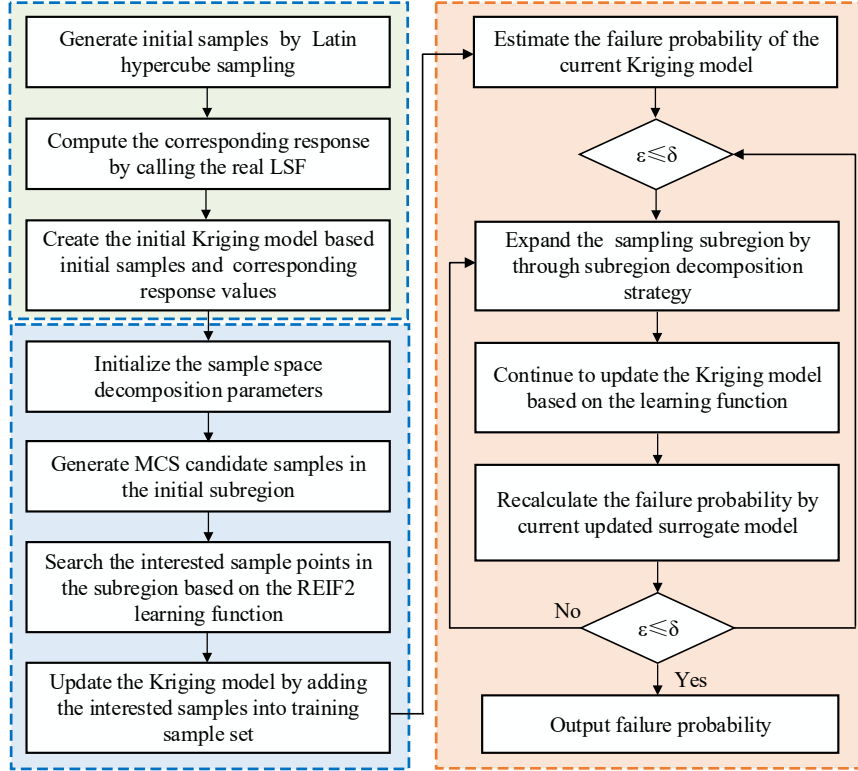


Fig. 2. Flowchart of the proposed AS-AK method.

Compared to conventional AK-MCS methods, the key advantage of the proposed AS-AK approach is the adaptive partitioning of the candidate sample space into concentric subregions. By separately managing the candidate sample size within each subregion, the AS-AK avoids the undesirable concentration of samples in certain areas, significantly enhancing both local approximation accuracy near critical failure boundaries and global convergence efficiency.

3. Collaborative multi-failure reliability framework with AS-AK

To efficiently handle reliability assessment of complex systems with multiple correlated failure modes, this section further proposes a collaborative multi-failure reliability analysis framework by integrating multiple adaptive subregion-based active Kriging surrogate model. Specifically, the proposed framework leverages a hierarchical collaborative modeling strategy [57-59], a linkage sampling technique [60-62], and the AS-AK surrogate modeling approach to systematically address the coupling and correlations among different failure modes. The key idea behind the proposed framework is to first

decompose a complex multi-failure system into multiple individual failure modes and establish independent AS-AK surrogate model for each mode. Then, the linkage sampling technique [63] is used to establish the accurate multi-failure reliability model by comprehensively considering the failure correlation among different failure modes. Therefore, the presented collaborative multi-failure reliability analysis framework can obtain the high-accuracy and high-efficiency in dealing with the multi-failure system reliability analysis.

Consider a system composed of p correlated failure modes, where $Y^{(p)}$ denotes the response of the p -th failure mode and $[Y^{(p)}]$ represents its allowable threshold [28]. The limit state function (LSF) for the p -th failure mode, $g^{(p)}(\mathbf{x})$, can be formulated as:

$$\begin{aligned}
 g^{(p)}(\mathbf{x}) &= [Y^{(p)}] - Y^{(p)} \\
 &= [Y^{(p)}] - f^T(\tilde{\mathbf{x}}^{(p)})\hat{\beta}^{(p)} \\
 &\quad + \mathbf{r}^T(\tilde{\mathbf{x}}^{(p)})[\mathbf{R}^{(p)}]^{-1}(Y_{max}^{(p)})
 \end{aligned} \tag{12}$$

where $\hat{\beta}^{(p)}$, $\mathbf{R}^{(p)}$, $\mathbf{r}^T(\tilde{\mathbf{x}}^{(p)})$, $f^T(\tilde{\mathbf{x}}^{(p)})$, $Y_{max}^{(p)}$, represent the regression coefficients, correlation model, correlation vector, regression basis function, and the maximum response in the AS-AK surrogate model of the p -th failure mode, respectively; \mathbf{E}

indicates the unit column vector.

For a system containing l correlated LSFs, the overall system failure probability P_{fs} can be expressed as:

$$P_{fs} = P(\cup_{p=1}^l g^{(p)}(x) \leq 0) \approx \frac{1}{N} \sum_{i=1}^N I_{Ft}(x_i) \quad (13)$$

where N is the total number of samples and the failure indicator function $I_{Ft}(x_i)$ is defined by:

$$I_F(x_i) = \begin{cases} 1, & \min_{p=1, \dots, l} g^{(p)}(x_i) \leq 0 \\ 0, & \text{else} \end{cases} \quad (14)$$

The variance and coefficient of variation (C.O.V.) of the estimated failure probability can be computed as follows:

$$V(\hat{P}_{fs}) = \frac{1}{N-1} \left[\frac{1}{N} \sum_{i=1}^N I_F(x_i) - \hat{P}_{fs}^2 \right] \quad (15)$$

$$\text{C.O.V.}(\hat{P}_{fs}) = \frac{\sqrt{V(\hat{P}_{fs})}}{\hat{P}_{fs}} \quad (16)$$

Generally, when the C.O.V. value is lower than 5%, the estimated failure probability is considered sufficiently accurate and stable. If the C.O.V. exceeds this threshold, additional candidate samples are adaptively generated, and the AS-AK surrogate model is updated iteratively until the convergence criterion (C.O.V. < 5%) is satisfied.

In summary, the proposed collaborative reliability framework strategically integrates multiple AS-AK surrogate models via hierarchical collaboration and linkage sampling techniques. It effectively addresses the computational challenge of multi-component, correlated failure modeling and efficiently approximates the highly nonlinear limit state functions for complex engineering systems. Consequently, the presented collaborative AS-AK framework achieves a high level of accuracy and computational efficiency, making it suitable for practical engineering reliability analyses involving multiple correlated failure modes.

4. Case studies

In this section, four representative numerical examples are selected to verify the effectiveness and computational advantages of the proposed AS-AK method. Specifically, these examples include a highly nonlinear bivariate function [55, 64], a ternary nonlinear function, a nonlinear oscillator system [51, 65], and a complex four-branch system [66-67]. To objectively evaluate the accuracy and efficiency of the proposed method, the reference failure probability obtained from a brute-force

Monte Carlo simulation with 1×10^6 samples is adopted as benchmarks.

4.1. Case I: a highly bivariate function

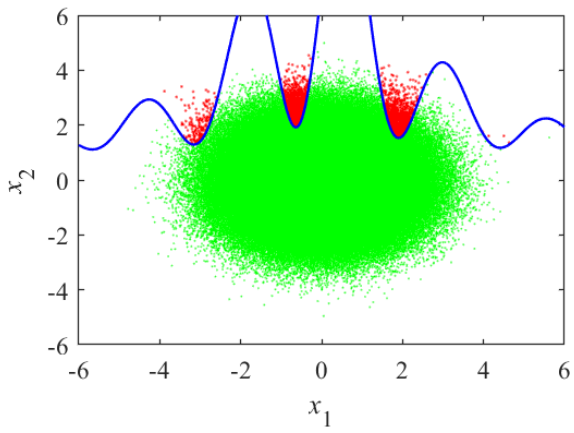
In this first example, a highly nonlinear performance function and limit state surface involving two independent random variables is considered. The explicit limit state function (LSF) is defined as:

$$G_1(x_1, x_2) = 1.2 - \frac{1}{20}(x_1^2 + 4)(x_2^2 - 1) + \sin(5x_1) \quad (17)$$

where x_1, x_2 follow independent standard normal distributions $x_1, x_2 \sim N(0,1)$. The failure domain is defined by $G_1(x_1, x_2) < 0$.

The distributions of candidate samples generated by the MCS and the proposed AS-AK method are presented in **Fig. 3**. Clearly, the candidate samples from the AS-AK method are uniformly distributed across the entire adaptive subregion, demonstrating efficient and balanced sample exploration. The modeling and updating process of the surrogate model using the AS-AK method is illustrated in **Fig. 4**. Herein, N_{call} denotes the total number of function calls; P_f represent the failure probability.

Table 1 summarizes the reliability analysis results obtained from different methods. It can be observed from **Fig. 4** and **Table 1** that the proposed AS-AK combined with REIF2 learning function method initially employed 14 Latin hypercube sampling samples to construct the initial Kriging model and subsequently iteratively selected 22 critical samples to refine the surrogate model. With only 36 total sample evaluations, the AS-AK achieved a failure probability estimation of 4.6×10^{-3} , precisely matching the reference solution obtained from 1×10^6 MCS samples. Compared to other learning functions (i.e., U, H, EFF), the REIF2 learning function demonstrates higher computational efficiency and accuracy. Compared with conventional Kriging and MCS methods, the AS-AK method significantly reduced computational efforts (fewer samples) while maintaining high accuracy. The convergence process curves of the failure probability and coefficient of variation shown in **Fig. 5** further verify the stability of the proposed method. Moreover, the adaptive subregion strategy ensured sufficient sample coverage near critical failure boundaries, further confirming the high efficiency and robustness of the proposed AS-AK method.

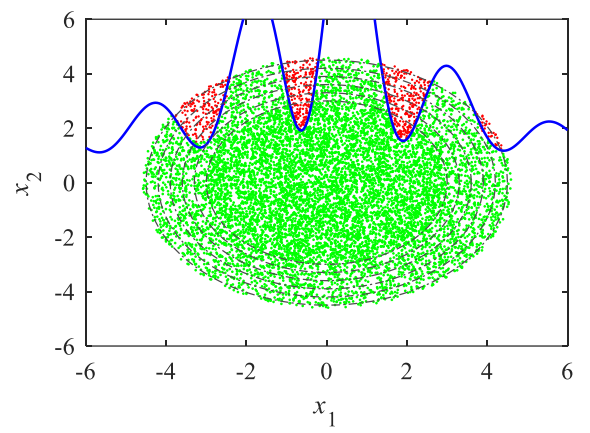


● Safety samples

● Failure samples

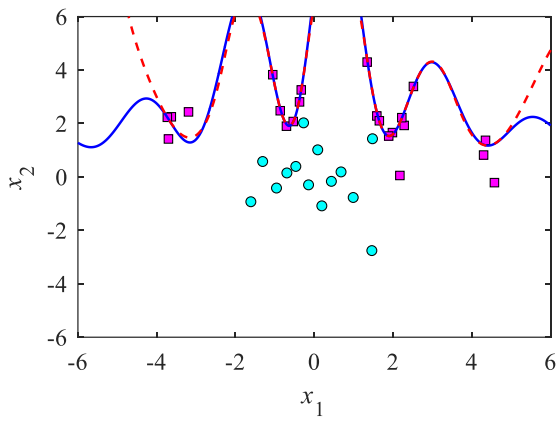
— True LSF

(a) MCS (10^6)

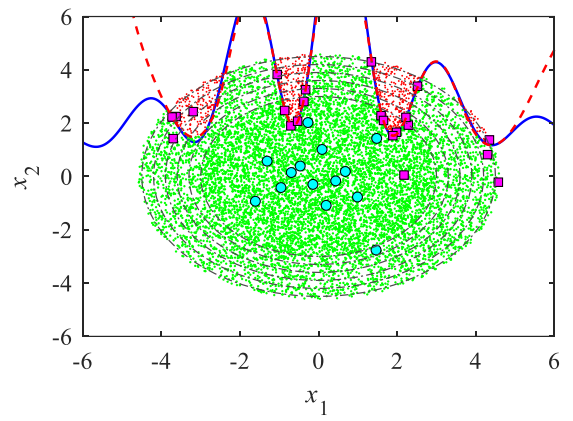


(b) AS-AK (10^4)

Fig. 3. Candidate pools generated with MCS, AS-AK for Case I.



(a) Fitted LSF



(b) Sampling distribution

● Initial samples

■ Add samples

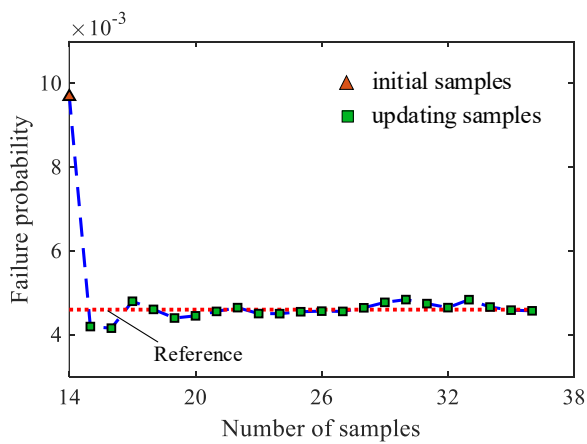
● Safety samples

● Failure samples

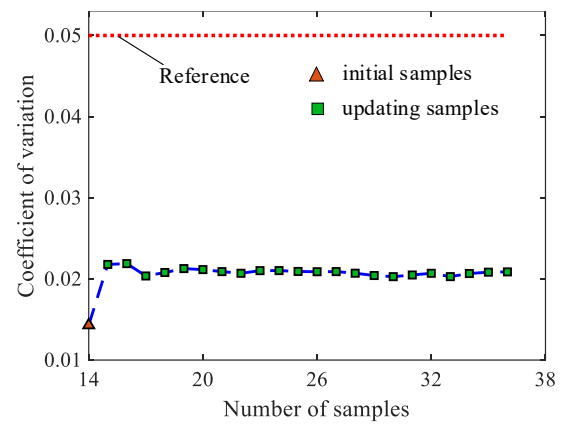
— True LSF

— Fitted LSF

Fig. 4. Modeling process for Case I.



(a) Failure probability



(b) Coefficient of variation

Fig. 5. The convergence process of failure analysis results for Case I.

Table 1. Results of failure probability for Case I.

Methods	N_{call}	P_f	Computing error
MCS	1×10^6	0.0046	-
Kriging	70	0.0048	4.35%
REIF2	31.7	0.0047	2.17%
MCMC	33	0.0047	2.17%
AK-MCS	37	0.0047	2.17%
AS-AK+U	62	0.0046	0
AS-AK+H	58	0.0046	0
AS-AK+EFF	65	0.0046	0
AS-AK+REIF2	36	0.0046	0

Note that the P_{MCS} , P_f indicate the failure probability of MCS method and surrogate model methods, respectively. Computing error of each surrogate model method is calculated by: $[(P_{MCS} - P_f) / P_{MCS}] \times 100\%$.

4.2. Case II: a ternary example

To further illustrate the effectiveness of the proposed AS-AK method in handling higher-dimensional nonlinear reliability problems, a three-dimensional nonlinear limit state function (LSF) is examined in this case study. The explicit form of the LSF is given by:

$$G_2(x_1, x_2, x_3) = \sin x_1 + 7 \sin^2 x_2 + 0.1 \sin x_3 \quad (18)$$

where x_1, x_2, x_3 are independent random variables with standard normal distribution, and the failure domain is defined by $G_2(x_1, x_2, x_3) < 0$.

Table 2 summarizes the computational results obtained by different reliability analysis methods. For the AS-AK combined with REIF2 learning function method, 21 initial samples with $x_1, x_2, x_3 \sim N(0, 1)$ generated by Latin hypercube sampling and corresponding responses calculated by the real LSF are used to construct the initial Kriging surrogate model. Subsequently, only 34 additional critical samples are adaptively selected through the active learning strategy, resulting in a total of 55 evaluations of the true performance function. The estimated failure probability by the AS-AK+REIF2 method closely matches the benchmark solution derived from the brute-force MCS with 1×10^6 samples.

Compared with the traditional Kriging method and AK-MCS method, which required significantly more samples to achieve comparable accuracy, the proposed AS-AK method demonstrates superior computational efficiency and accuracy.

These results further validate that the AS-AK approach is highly suitable for efficiently and accurately addressing reliability assessment problems involving high dimensionality and strong nonlinearity.

Table 2. Results of failure probability for Case II.

Methods	N_{call}	P_f	Computing error
MCS	1×10^6	0.1107	-
Kriging	106	0.1110	0.27%
AK-MCS	120	0.1108	0.09%
AS-AK+U	60	0.1083	2.17%
AS-AK+H	81	0.1115	0.72%
AS-AK+EFF	99	0.1084	2.08%
AS-AK+REIF2	55	0.1107	0

4.3. Case III: a nonlinear oscillator system

In this example, the reliability of a nonlinear spring oscillator subjected to rectangular pulse excitation is investigated to demonstrate the efficiency and accuracy of the proposed AS-AK method in complex dynamic engineering systems. The schematic representation of the nonlinear oscillator system is illustrated in **Fig. 6**, and six normal distributed variables are considered. The corresponding statistical characteristics of the six independent random variables are summarized in **Table 3**. The explicit limit state function is defined as follows:

$$G_3(S, F_1, M, k_1, k_2, t_1) = 3S - \left| \frac{2F_1}{M\omega^2} \sin\left(\frac{\omega t_1}{2}\right) \right|, \omega = \frac{\sqrt{k_1+k_2}}{M} \quad (19)$$

The results of reliability analyses obtained from different methods are summarized in **Table 4**. For the proposed AS-AK combined with REIF2 learning function method, an initial surrogate model is constructed using 42 Latin hypercube samples, followed by the adaptive selection of 80 additional critical samples via active learning. Thus, only 122 evaluations of the original complex nonlinear performance function were required to achieve an accurate estimation of the failure probability ($P_f=0.0586$). Compared with other learning functions (i.e., U, H, EFF), this result closely aligns with the benchmark solution ($P_f=0.0587$) derived from the brute-force MCS approach using 1×10^6 samples.

In contrast, the traditional Kriging surrogate model and AK-MCS method require 256 and 165 performance function evaluations to achieve comparable accuracy ($P_f=0.0583$ and $P_f=0.0609$), respectively. Therefore, the AS-AK method clearly

demonstrates superior computational efficiency, significantly reducing the required number of function evaluations while maintaining high reliability estimation accuracy. This case further confirms that the proposed AS-AK approach is

particularly suitable for solving complex reliability analysis problems characterized by dynamic and strongly nonlinear behaviors.

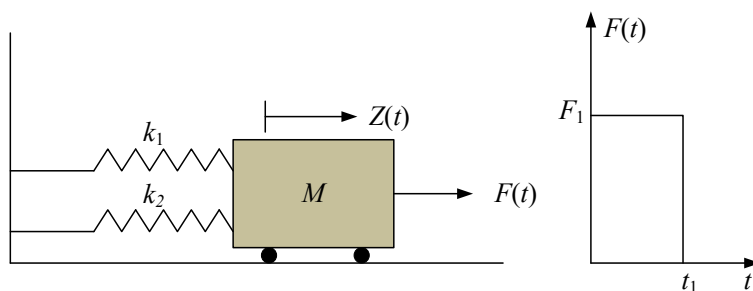


Fig. 6. A nonlinear oscillator.

Table 3. Parameter distribution characteristics of Case III.

Variables	Distribution type	Mean	Standard deviation
S	Normal distribution	0.5	0.1
F_1	Normal distribution	0.8	0.15
M	Normal distribution	1	0.05
t_1	Normal distribution	1	0.15
k_1	Normal distribution	1	0.1
k_2	Normal distribution	0.1	0.1

Table 4. Results of failure probability for Case III.

Methods	N_{call}	P_f	Computing error
MCS	1×10^6	0.0587	-
Kriging	256	0.0583	0.68%
AK-MCS	165	0.0609	3.75%
AS-AK+U	159	0.0621	5.79%
AS-AK+H	202	0.0519	11.58%
AS-AK+EFF	175	0.0628	6.98%
AS-AK+REIF2	122	0.0586	0.17%

4.4. Case IV: a four branches system

The fourth numerical example involves a complex performance function characterized by four distinct nonlinear branches, representing typical challenges encountered in engineering system reliability analysis. It has four branches, and the explicit expression of this limit state function is given as:

$$G_4(x_1, x_2) = \begin{cases} 4 + 0.1(x_1 - x_2)^2 - \frac{(x_1 + x_2)}{\sqrt{2}} \\ 4 + 0.1(x_1 - x_2)^2 + \frac{(x_1 + x_2)}{\sqrt{2}} \\ \frac{7}{\sqrt{2}} + (x_1 - x_2) \\ \frac{7}{\sqrt{2}} - (x_1 - x_2) \end{cases} \quad (20)$$

where x_1 and x_2 are independent standard Gaussian random

variables. Failure domain is defined by $G_4(x_1, x_2) \leq 0$.

Fig. 7 compares the distributions of candidate samples generated by the traditional MCS and the proposed AS-AK method. As clearly shown in **Fig. 7**, candidate samples from the AS-AK method exhibit a more uniform and effective distribution near the critical limit state boundaries, demonstrating the method's capability for efficient exploration and accurate approximation in critical regions with relatively fewer samples. **Fig. 8** illustrates the iterative surrogate modeling and updating process employed by the AS-AK method. As revealed in **Fig. 8**, 14 samples are used to construct initial Kriging model, extra 15 samples are selected to update Kriging model. After 29 real LSF calls, the Kriging fitted LSF approximates the real LSF. **Table 5** summarizes the reliability analysis results obtained using different methods. Remarkably, the proposed AS-AK combined with REIF2 learning function method achieves a highly accurate failure probability estimate (4.81×10^{-4}) using only 29 calls to the real limit state function, resulting in an extremely low relative error of only 0.21% compared with the benchmark MCS solution (based on 1×10^6 samples).

In contrast, other comparative methods such as traditional

Kriging, REIF2, Markov chain Monte Carlo (MCMC), and AK-MCS require significantly more function evaluations to achieve comparable accuracy. This further validates the superior computational efficiency and high accuracy of the AS-AK

method, particularly suitable for reliability analyses involving systems with highly nonlinear and multiple-branch limit state functions.

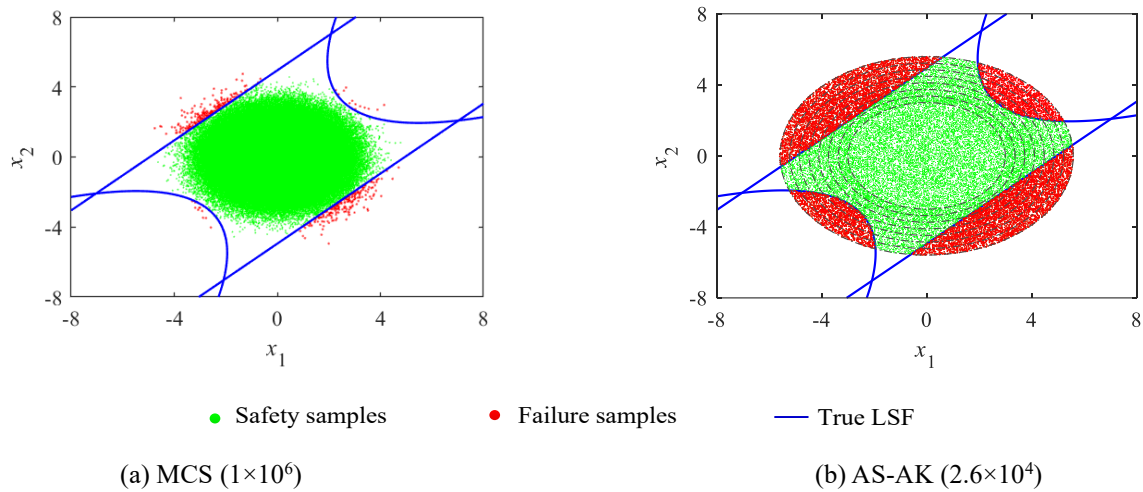


Fig. 7. Candidate pools generated with MCS, AS-AK for Case IV.

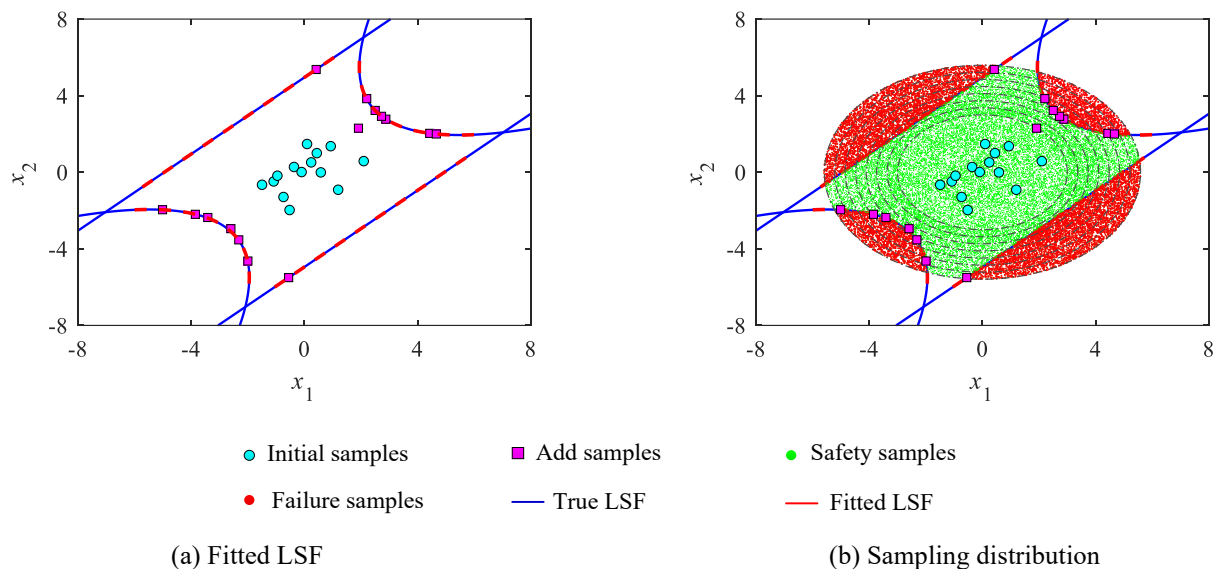


Fig. 8. Modeling process for Case IV.

Table 5. Results of failure probability for Case IV.

Methods	N_{call}	P_f	Computing error
MCS	1×10^6	4.8×10^{-4}	-
Kriging	160	4.42×10^{-4}	7.92%
REIF2	68.8	5.11×10^{-4}	6.46%
MCMC	56.3	5.11×10^{-4}	6.46%
MRIS	55.4	5.10×10^{-4}	6.25%
AK-MCS	59	5.09×10^{-4}	6.04%
AS-AK+U	43	4.89×10^{-4}	1.88%
AS-AK+H	68	4.86×10^{-4}	1.25%
AS-AK+EFF	66	4.87×10^{-4}	1.46%
AS-AK+REIF2	29	4.81×10^{-4}	0.21%

5. Engineering application: rigid-flexible coupling system

In aeroengine rigid-flexible coupling systems, accurate adjustment and synchronization of stator blade rotation angles are crucial for ensuring stable and efficient compressor operation. However, due to inherent uncertainties such as variability in material properties, dimensional tolerances, loading conditions, and the flexible deformation effects in key components (e.g., rocker arms and linkage rings), the actual rotation angles of stator blades frequently deviate from their design targets. These deviations significantly compromise motion accuracy, posing substantial risks to the reliability and safety of aeroengines. To verify the effectiveness and practical

applicability of the proposed AS-AK method, a detailed reliability assessment of an aeroengine rigid-flexible coupling system is conducted in this section. **Fig. 9** shows the schematic diagram of aeroengine rigid-flexible coupling systems. In the process of mechanism simulation, the flexibility of rocker arm components is carried out by using finite element software. The specific finite element method (FEM) discretization parameters are as follows: TC4 Material, Number of modes 24, Node=425, Elements=1321, RBE2 rigid attachment. The boundary conditions are as follows: the aerodynamic force of the blade body is 500N, the axial force of the inner ring is 200N, the aerodynamic moment is 1000N.mm, and the driving speed is 80mm/s. The process of one-time deterministic rigid-flexible co-simulation (that is, the real LSF in this project) of the mechanism is as follows: Firstly, the rigid body model is constructed and the motion pair and load are defined in the dynamics software, and then the flexible body modal neutral file (MNF) is generated in the finite element software and the corresponding rigid parts are replaced by importing the MNF. Then, the rigid-flexible body load and motion transmission are realized through RBE2/RBE3 connection, and the kinematic and dynamic analysis of the mechanism is completed. Finally, the blade rotation angle is extracted, and the average angle, maximum angle and minimum angle of each blade can be obtained by calculation.

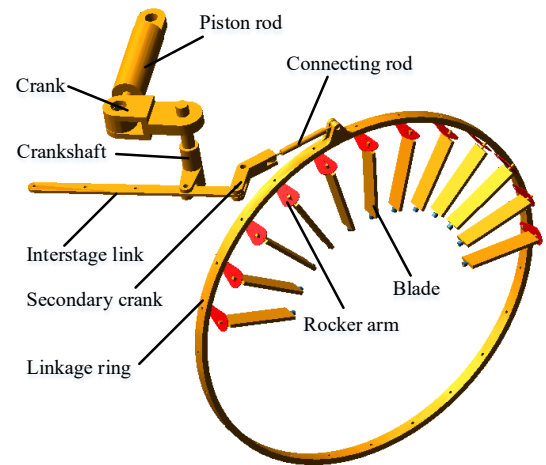


Fig. 9. Schematic diagram of aeroengine rigid-flexible coupling systems.

5.1. Material preparations

In this case study, two primary failure modes related to motion accuracy of the rigid-flexible coupling system are investigated: (1) insufficient average rotation angle of the stator blades, and (2) excessive variation between maximum and minimum rotation angles among individual stator blades. These two failure modes represent common reliability challenges encountered in practical engineering applications. The limit state function describing these failure modes are mathematically formulated as follows:

$$G(x) = \begin{cases} |\alpha(x_{11}, x_{12}, \dots, x_{ln})_{ave} - \alpha_1| < \delta_1, & \text{(average rotation angle failure)} \\ |\alpha(x_{21}, x_{22}, \dots, x_{mn})_{err} - \alpha_2| < \delta_2, & \text{(rotation angle variation failure)} \end{cases} \quad (21)$$

where $\alpha(x_{11}, x_{12}, \dots, x_{ln})_{ave}$ is the average rotation angle of stator blades, obtained through rigid-flexible coupling simulations; α_1 the design target angle (set as 34.67°), and δ_1 the allowable deviation threshold for the average rotation angle (set as 1.5°). Similarly, $\alpha(x_{21}, x_{22}, \dots, x_{mn})_{err}$ represents the maximum minimum angle error among the blades obtained from simulations; α_2 is the target limit for acceptable variation (set as 0.24°), and δ_2 is the allowable threshold for this angle variation (set as 0). The input random variables associated with the average rotation angle failure mode ($x_{11}, x_{12}, \dots, x_{ln}$) and rotation

angle variation failure mode ($x_{21}, x_{22}, \dots, x_{mn}$) are assumed independent and normally distributed. The statistical characteristics and parameter distributions of these variables are detailed in **Tables 6** and **7**, respectively. Noted that the parameters range of the input variables is determined by the specified engineering tolerance and allowable variation in the product design and manufacturing stages. Moreover, the standard deviation of the input variables can be calculated from the corresponding upper and lower tolerance boundaries according to the “ 3σ principle” of normal distribution.

Table 6. Distribution parameters of input random variables with average angle.

Parameter name	Parameter range	Distribution type	Standard deviation
Driving speed peak x_{11} (mm/s)	[-81, -79]	Normal distribution	0.334
Secondary crank angle x_{12} ($^\circ$)	[134.75, 135.25]	Normal distribution	0.0834
Crankshaft length x_{13} (mm)	[49.938, 50.062]	Normal distribution	0.021

Parameter name	Parameter range	Distribution type	Standard deviation
Secondary crank length 1 x_{14} (mm)	[49.938,50.062]	Normal distribution	0.021
Interstage link length x_{15} (mm)	[79.926,80.074]	Normal distribution	0.029
Secondary crank length 2 x_{16} (mm)	[49.938,50.062]	Normal distribution	0.021
Piston rod length x_{17} (mm)	[199.9,200.1]	Normal distribution	0.0334
Crank length x_{18} (mm)	[99.913,100.087]	Normal distribution	0.029
Connecting rod length x_{19} (mm)	[114.913,115.087]	Normal distribution	0.029
Rocker arm length x_{20} (mm)	[39.938,40.062]	Normal distribution	0.021

Table 7. Distribution parameters of input random variables with maximum minimum angle error.

Parameter name	Parameter range	Distribution type	Standard deviation
Crankshaft height x_{21} (mm)	[99.913,100.087]	Normal distribution	0.029
Connecting rod length x_{22} (mm)	[114.913,115.087]	Normal distribution	0.029
Piston rod length x_{23} (mm)	[199.9,200.1]	Normal distribution	0.0334
Crank length x_{24} (mm)	[99.913,100.087]	Normal distribution	0.029
Secondary crank length 2 x_{25} (mm)	[49.937,50.063]	Normal distribution	0.021
Interstage link length x_{26} (mm)	[79.926,80.074]	Normal distribution	0.029
Crankshaft length x_{27} (mm)	[49.938,50.063]	Normal distribution	0.021
Secondary crank length 1 x_{28} (mm)	[49.938,50.063]	Normal distribution	0.021

5.2. AS-AK surrogate modeling

According to the statistical characteristics of the input random variables summarized in **Table 6**, an initial training set consisting of 70 samples is generated using LHS. These samples are subsequently imported into the rigid-flexible coupling simulation model to obtain the corresponding average rotation angle responses. Based on these initial samples, an initial AS-AK surrogate model is constructed. To enhance the accuracy and efficiency of the surrogate model, an additional 45 critical samples are iteratively selected and updated through the adaptive subregion decomposition and active learning strategy described earlier. After conducting a total of 115 rigid-flexible coupling simulations (70 initial plus 45 adaptive samples in **Tables 6**), a highly accurate AS-AK surrogate model for predicting the average rotation angle is successfully established.

Similarly, considering the statistical characteristics of input variables related to the maximum minimum angle error as shown in **Table 7**, 70 sets of initial input samples are generated by LHS. These samples are sequentially introduced into the rigid-flexible coupling simulation to determine the corresponding maximum minimum angle error responses (α_{err}). Following this initial stage, an additional 130 critical samples are selected adaptively to iteratively refine the surrogate model. Consequently, through 200 total simulations (70 initial plus 130 adaptive samples), a precise AS-AK surrogate model for predicting the maximum rotation angle error is obtained.

Finally, by employing the linkage sampling technique, the two independently developed surrogate models-one for the average rotation angle and the other for the maximum minimum angle error-are integrated into a collaborative AS-AK reliability surrogate model.

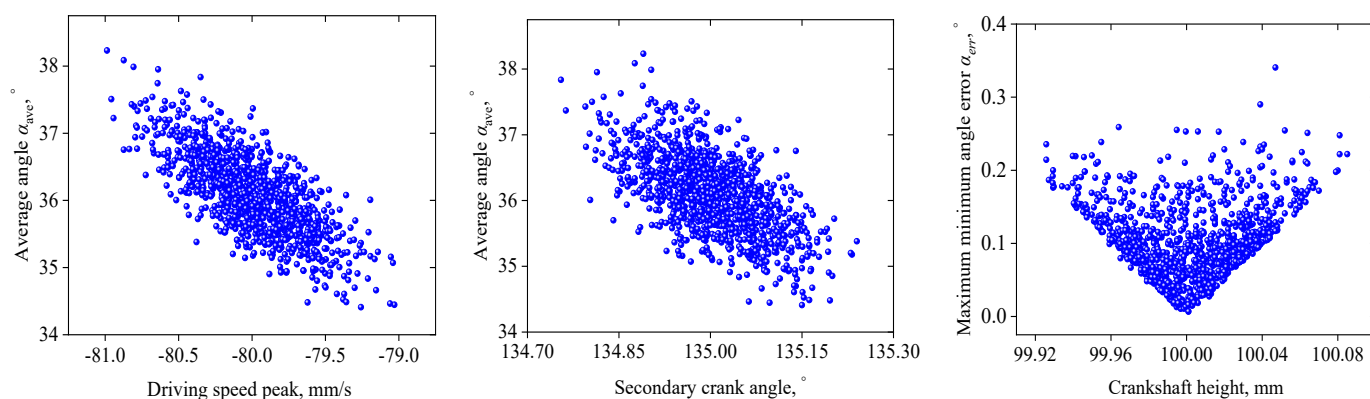


Fig. 10. Scatter sketches of sensitive variables.

This collaborative surrogate model accurately accounts for both failure modes simultaneously, effectively capturing their potential correlations and interactions. **Fig. 10** shows the scatter plots illustrating relationships between the input variables and the corresponding output responses obtained by the established surrogate model. As demonstrated in **Fig. 10**, there exist clear and strong correlations between certain input variables and blade adjustment angles. These results indicate the highly nonlinear nature of the rigid-flexible coupling system, emphasizing the necessity and advantage of employing the proposed AS-AK surrogate method for reliability and sensitivity analyses.

5.3. Reliability analysis

To efficiently quantify the reliability of the aeroengine rigid-flexible coupling system, 10,000 samples are generated via Latin hypercube sampling and subsequently analyzed using the established collaborative AS-AK surrogate model. By employing the surrogate model rather than conducting computationally expensive rigid-flexible coupling simulations,

we rapidly obtain precise probability distributions for both the average rotation angle and the maximum minimum angular variation of the stator blades.

Figs. 11 and **12** illustrate the probability distribution results obtained from the AS-AK surrogate model. Specifically, **Fig. 12** indicates that the average rotation angle of the stator blades closely follows a normal distribution. Under the given precision requirement (allowable deviation threshold $\delta_1=1.5^\circ$), the reliability associated with maintaining the average rotation angle within the acceptable range reaches approximately 99.91%. Meanwhile, the maximum angular error among the blades follows a lognormal distribution. Here, PDF represents probability density function (PDF), CDF denotes cumulative distribution function (CDF). When the precision design criterion is set to an allowable angle variation $\alpha_2=0.24^\circ$, the corresponding reliability reaches approximately 99.96%. These high reliability levels illustrate that the proposed collaborative AS-AK model effectively meets the stringent reliability requirements typically imposed on aeroengine rigid-flexible coupling systems.

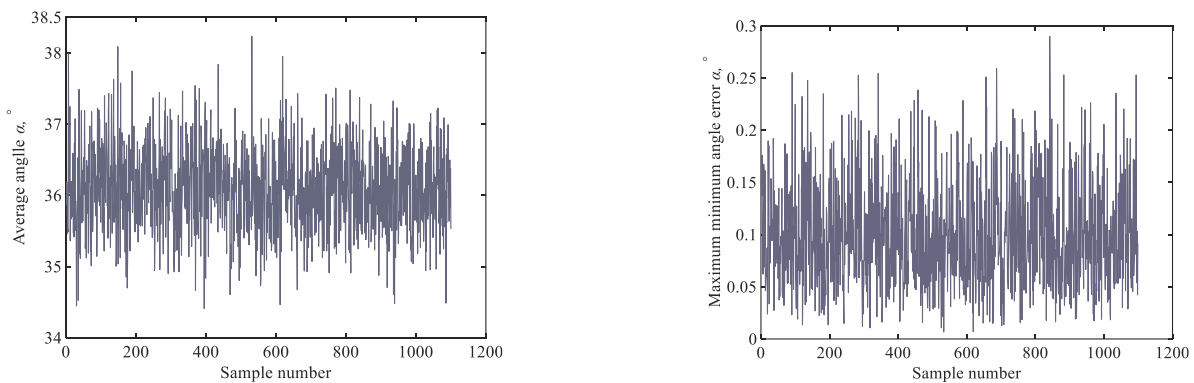


Fig. 11. Iteration history of AS-AK model.

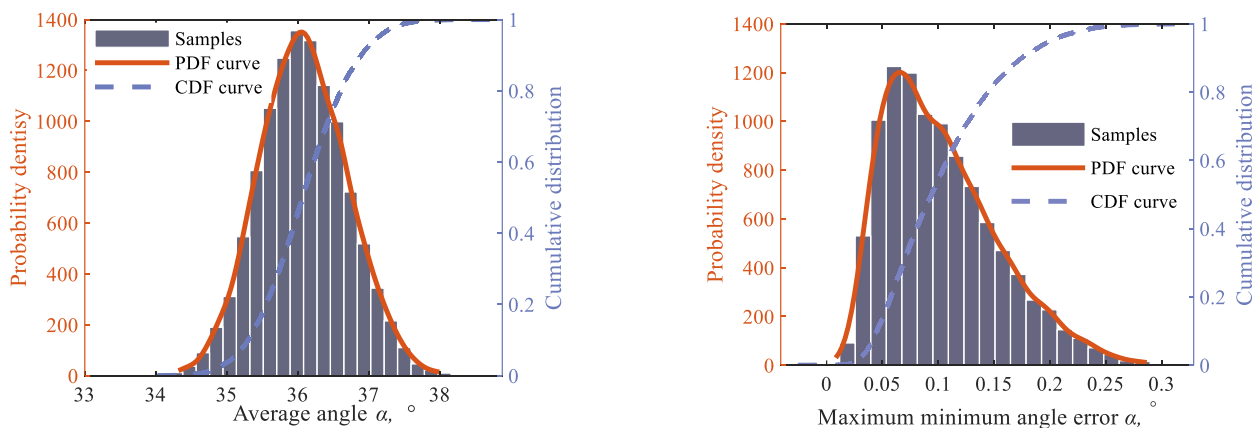


Fig. 12. Iteration curve of AS-AK model.

5.4. Post-validation of AS-AK

To comprehensively validate the computational effectiveness and accuracy of the proposed AS-AK method, a comparative analysis is conducted by employing three commonly used methods, the traditional Kriging, AK-SYS, and MCS method. The comparative reliability assessment results for the aeroengine rigid-flexible coupling system are presented in **Table 8**. In reliability analysis, fewer function evaluations typically correlate with reduced computational cost and higher efficiency. The coefficient of determination (R^2) and RMSE (Root Mean Squared Error) are used here as a quantitative indicator of surrogate model accuracy. As shown in **Table 8**, the AS-AK surrogate model requires only 315 calls to the real rigid-flexible coupling simulation model, significantly fewer than the 500 calls required by the traditional Kriging approach and 395 calls by the AK-SYS method. Moreover, the AS-AK surrogate achieves a higher R^2 value and a smaller RMSE value, indicating superior predictive accuracy compared to traditional Kriging. The estimated failure probability obtained by AS-AK also exhibits a lower computational error relative to the reference MCS solution, further highlighting its improved precision.

Therefore, this comparative analysis clearly demonstrates that the proposed AS-AK method substantially outperforms traditional Kriging, AK-SYS, and MCS approaches, providing robust computational benefits in terms of both accuracy and efficiency for reliability analysis in complex engineering systems.

Table 8. Results of failure probability for mechanism.

Methods	N_{call}	P_f	Computing error	R^2	RMSE
MCS	10000	0.0127	-	-	-
Kriging	500	0.0151	18.90%	0.9144	0.0147
AK-SYS	395	0.0134	5.51%	0.9151	0.0146
AS-AK	315	0.0130	2.36%	0.9759	0.0113

6. Conclusions

This paper proposes an Adaptive Subregion-based Active Kriging (AS-AK) surrogate modeling method to efficiently evaluate the reliability of complex engineering systems involving multiple correlated failure modes, high nonlinearity, and small failure probability. The proposed AS-AK method

integrates an adaptive subregion decomposition strategy with active learning-based Kriging modeling to significantly enhance computational accuracy and efficiency. Moreover, a collaborative multi-failure reliability analysis framework is developed by incorporating multiple AS-AK surrogate models, systematically capturing the correlations and interactions among various failure modes. Four benchmark numerical examples and a practical engineering case involving an aeroengine rigid-flexible coupling system are thoroughly analyzed to validate the proposed method. The main conclusions are as follows:

(1) The proposed AS-AK method demonstrates significant improvements over traditional reliability methods in computational efficiency and accuracy, notably reducing the required evaluations of costly real limit state functions. These advantages become more pronounced as problem complexity and nonlinearity increase, achieving results closely aligned with extensive Monte Carlo simulations.

(2) The adaptive subregion decomposition strategy embedded in AS-AK effectively improves sampling efficiency and reduces redundancy. Additionally, the collaborative multi-failure framework significantly simplifies surrogate modeling complexity and enhances accuracy, efficiently addressing reliability problems with correlated and multimodal failure modes.

(3) Successful applications to multiple benchmark examples and a complex engineering system highlight the robustness and effectiveness of the AS-AK method. This approach offers valuable theoretical insights and practical analytical tools for reliability-oriented design and optimization of complex interconnected engineering systems. In the follow-up work, to further verify the superiority of the proposed method, the sensitivity analysis of some key parameters in the proposed method would be studied. Meanwhile, to further extend the applications of the proposed method in more complex problem (i.e., highly nonlinear functions, high-dimensional uncertain variables, etc.), the Markov Chain Monte Carlo (MCMC) and subset simulation method will be further combined.

Acknowledgements

This paper is co-supported by the National Natural Science Foundation of China (Grant 52105136), the Basic and Applied Basic Research Foundation of Guangdong Province (Grant no. 2024A1515240025), Suqian Science & Technology Program (Grant No. K202444) and Suqian College Talent Introduction and Research Start up Fund (Grant No. 106-CK00042/160). The authors would like to thank them.

References

1. Cheng YX, Zhou Z, Wang KL, Wang Y. Design and optimization of a transmission mechanism developed for distributed electric propulsion aircraft, *Aerospace Science and Technology*, 2022, 127: 107714.
2. Cai W, Ma Q, Wang Y, Gan X. Crashworthiness analysis and multi-objective optimization of Al/CFRP hybrid tube with initial damage under transverse impact, *Polymer Composites*, 2023, 44(11): 7953-7971. <https://doi.org/10.1002/pc.27678>
3. Song LK, Tao F, Choy Y, Yang LC, Wei YF. Cascade sampling-driven block mapping for coupled reliability evaluation of turbine cooling systems, *Mechanical Systems and Signal Processing*, 2025, 236: 113008.
4. Ma Q, Dong B, Zha Y, Sun J, Gan X, Cai M, Zhou T. Multi-objective optimization for energy absorption of carbon fiber-reinforced plastic/aluminum hybrid circular tube under both transverse and axial loading, *Journal of Materials Engineering and Performance*, 2020, 29(9): 5609-5624. <https://doi.org/10.1007/s11665-020-04941-4>
5. Wang S, Ma QH, Gan XH, Zhou TJ. Crashworthiness analysis and multi-objective optimization of Al/CFRP tubes with induced holes, *Polymer Composites*, 2021, 42(10): 5280-5299. <https://doi.org/10.1002/pc.26222>
6. Song LK, Tao F, Li XQ, et al. Physics-embedding multi-response regressor for time-variant system reliability assessment, *Reliability Engineering & System Safety*, 2025, 263: 111262.
7. Li XQ, Song LK, Bai GC. Deep learning regression-based stratified probabilistic combined cycle fatigue damage evaluation for turbine bladed disks, *International Journal of Fatigue*, 2022, 159: 106812.
8. Ma Q, Zha Y, Dong B, Gan X. Structure design and multiobjective optimization of CFRP/aluminum hybrid crash box, *Polymer Composites*, 2020, 41(10): 4202-4220. <https://doi.org/10.1002/pc.25705>
9. Qin X, Ma Q, Gan X, Cai M, Cai W. Failure analysis and multi-objective optimization of crashworthiness of variable thickness Al-CFRP hybrid tubes under multiple loading conditions, *Thin-Walled Structures*, 2023, 184: 110452.
10. Gordini M, Habibi MR, Taviana MH, TahamouliRoudsari M, Amiri M. Reliability analysis of space structures using Monte-Carlo simulation method, *Structures*, 2018, 14: 209-219. <https://doi.org/10.1016/j.istruc.2018.03.011>
11. Razaaly N, Congedo PM. Extension of AK-MCS for the efficient computation of very small failure probabilities, *Reliability Engineering and System Safety*, 2020, 203: 107084.
12. Zhang H, Song LK, Bai GC. Moving-zone renewal strategy combining adaptive Kriging and truncated importance sampling for rare event analysis, *Structural and Multidisciplinary Optimization*, 2022, 65: 285. <https://doi.org/10.1007/s00158-022-03398-4>
13. Lim J, Lee B, Lee I. Post optimization for accurate and efficient reliability-based design optimization using second-order reliability method based on importance sampling and its stochastic sensitivity analysis, *International Journal for Numerical Methods in Engineering*, 2016, 107(2): 93-108. <https://doi.org/10.1002/nme.5150>
14. Jiang X, Lu Z. Extended fuzzy first-order and second-moment method based on equivalent regularization for estimating failure credibility, *Aerospace Science and Technology*, 2022, 124: 107559.
15. Zhu SP, Keshtegar B, Ben Seghier MEA, Zio E, Taylan O. Hybrid and enhanced PSO: Novel first order reliability method-based hybrid intelligent approaches, *Computer Methods in Applied Mechanics and Engineering*, 2022, 393: 114730.
16. Song LK, Bai GC, Li XQ, Wen J. A unified fatigue reliability-based design optimization framework for aircraft turbine disk, *International Journal of Fatigue*, 2021, 152: 106422.
17. Lelièvre N, Beaurepaire P, Mattrand C, Gayton N. AK-MCSi: A Kriging-based method to deal with small failure probabilities and time-consuming models, *Structural Safety*, 2018, 73: 1-11. <https://doi.org/10.1016/j.strusafe.2018.01.002>
18. Li XQ, Song LK, Bai GC. Recent advances in reliability analysis of aeroengine rotor system: a review, *International Journal of Structural Integrity*, 2022, 13(1): 1-29. <https://doi.org/10.1108/IJSI-10-2021-0111>

19. Li XQ, Song LK, Bai GC, Li DG. Physics-informed distributed modeling for CCF reliability evaluation of aeroengine rotor systems, *International Journal of Fatigue*, 2022, 167: 107342.
20. Wei JB, Liu ZJ, Sun YH, Wang XB. An active learning method for structural reliability combining response surface model with Gaussian process of residual fitting and reliability-based sequential sampling design, *Eksploatacja i Niezawodność – Maintenance and Reliability*, 2025, 27(1): 193443.
21. Song LK, Li XQ, Zhu SP, Choy YS. Cascade ensemble learning for multi-level reliability evaluation, *Aerospace Science and Technology*, 2024, 148: 109101.
22. Song LK, Choy YS, Zhang S, Wang BL. Multi-XGB: A multi-objective reliability evaluation approach for aeroengine turbine discs, *Digital Engineering*, 2024, 2: 100006.
23. Gao HF, Wang YH, Xu JJ, Qin HB. Fatigue strength reliability assessment of turbofan blades subjected to intake disturbances based on the improved kriging model, *Eksploatacja i Niezawodność - Maintenance and Reliability*, 2025, 27(2): 194175.
24. Wang ER, Wu X, Liu D, Wang SP, Shang YX. Artificial neural network supported monotonic stochastic processes for reliability analysis considering multi-uncertainties, *Eksploatacja i Niezawodność - Maintenance and Reliability*, 2025, 27(3): 197051.
25. Gaspar B, Teixeira AP, Soares CG. Adaptive surrogate model with active refinement combining Kriging and a trust region method, *Reliability Engineering and System Safety*, 2017, 165: 277-291. <https://doi.org/10.1016/j.res.2017.03.035>
26. Zhang H, Song LK, Bai GC. Active extremum Kriging-based multi-level linkage reliability analysis and its application in aeroengine mechanism systems, *Aerospace Science and Technology*, 2022, 131: 107968.
27. Moustapha M, Marelli S, Sudret B. Active learning for structural reliability: Survey, general framework and benchmark, *Structural Safety*, 2022, 96: 102174.
28. Zhang H, Song LK, Bai GC, Li XQ. Fatigue reliability framework using enhanced active Kriging-based hierarchical collaborative strategy, *International Journal of Structural Integrity*, 2023, 14(2): 267-292. <https://doi.org/10.1108/IJSI-09-2022-0116>
29. Luo CQ, Zhu SP, Keshtegar B, Macek W, Branco R, Meng DB. Active Kriging-based conjugate first-order reliability method for highly efficient structural reliability analysis using resample strategy, *Computer Methods in Applied Mechanics and Engineering*, 2024, 423: 116863.
30. Thompson T, McMullen R, Nemani V, Hu Z, Hu C. A comparative study of acquisition functions for active learning kriging in reliability-based design optimization, *Structural and Multidisciplinary Optimization*, 2025, 68(3): 1-40. <https://doi.org/10.1007/s00158-025-03978-0>
31. Zhou T, Peng Y. A new active-learning function for adaptive Polynomial-Chaos Kriging probability density evolution method, *Applied Mathematical Modelling*, 2022, 106: 86-99. <https://doi.org/10.1016/j.apm.2022.01.030>
32. Meng D, Yang H, Yang S, Zhang Y, De Jesus AM, Correia J, Fazeres-Ferradosa T, Macek W, Branco R, Zhu SP. Kriging-assisted hybrid reliability design and optimization of offshore wind turbine support structure based on a portfolio allocation strategy, *Ocean Engineering*, 2024, 295: 116842.
33. Meng D, Yang S, De Jesus AM, Fazeres-Ferradosa T, Zhu SP. A novel hybrid adaptive Kriging and water cycle algorithm for reliability-based design and optimization strategy: Application in offshore wind turbine monopile, *Computer Methods in Applied Mechanics and Engineering*, 2023, 412: 116083.
34. Meng D, Yang S, De Jesus AM, Zhu SP. A novel Kriging-model-assisted reliability-based multidisciplinary design optimization strategy and its application in the offshore wind turbine tower, *Renewable Energy*, 2023, 203: 407-420. <https://doi.org/10.1016/j.renene.2022.12.062>
35. Yang XF, Zhang Y, Wang T, Zhang HZ. An active learning reliability method combining population Monte Carlo and Kriging model for small failure probability, *Structures*, 2024, 70: 107621.
36. Echard B, Gayton N, Lemaire M. AK-MCS: An active learning reliability method combining Kriging and Monte Carlo Simulation, *Structural Safety*, 2011, 33(2): 145-154. <https://doi.org/10.1016/j.strusafe.2011.01.002>
37. De Angelis M, Patelli E, Beer M. Advanced line sampling for efficient robust reliability analysis, *Structural safety*, 2015, 52: 170-182. <https://doi.org/10.1016/j.strusafe.2014.10.002>
38. Wang J, Lu Z, Wang L. An efficient method for estimating failure probability bounds under random-interval mixed uncertainties by

- combining line sampling with adaptive Kriging, *International Journal for Numerical Methods in Engineering*, 2023, 124(2): 308-333. <https://doi.org/10.1002/nme.7122>
39. Dang C, Valdebenito MA, Faes MG, Song J, Wei P, Beer M. Structural reliability analysis by line sampling: A Bayesian active learning treatment, *Structural Safety*, 2023, 104: 102351.
 40. Frank G. An adaptive directional importance sampling method for structural reliability, *Probabilistic Engineering Mechanics*, 2011, 26: 134-141. <https://doi.org/10.1016/j.probengmech.2010.11.002>
 41. Guo Q, Liu YS, Chen BQ, et al. An active learning Kriging model combined with directional importance sampling method for efficient reliability analysis, *Probabilistic Engineering Mechanics*, 2020, 60: 103054.
 42. Grooteman F. Adaptive radial-based importance sampling method for structural reliability, *Structural Safety*, 2008, 30: 533-542. <https://doi.org/10.1016/j.strusafe.2007.10.002>
 43. Dubourg V, Sudret B, Bourinet JM. Reliability-based design optimization using Kriging surrogates and subset simulation, *Structural and Multidisciplinary Optimization*, 2011, 44(5): 673-690. <https://doi.org/10.1007/s00158-011-0653-8>
 44. Zhao Z, Lu ZH, Zhao YG, Xu TF, Zhang YF. A novel random-interval hybrid reliability analysis method combining active learning Kriging and two-phase subset simulation, *Structures*, 2024, 63: 106383.
 45. Wang T, Chen Z, Li G, He J, Shi R, Liu C. Adaptive Kriging-based probabilistic subset simulation method for structural reliability problems with small failure probabilities, *Structures*, 2024, 70: 107726.
 46. Soubra AH, Al-Bittar T, Thajeel J, et al. Probabilistic analysis of strip footings resting on spatially varying soils using kriging metamodeling and importance sampling, *Computers and Geotechnics*, 2019, 114: 103107.
 47. Gao HF, Wang AJ, Zio E, Bai GC. An integrated reliability approach with improved importance sampling for low-cycle fatigue damage prediction of turbine disks, *Reliability Engineering and System Safety*, 2020, 199: 106819.
 48. Dong S, Li L, Yuan T, Yu X, Wang P, Jia F. A random interval coupling-based active learning Kriging with meta-model importance sampling method for hybrid reliability analysis under small failure probability, *Computer Methods in Applied Mechanics and Engineering*, 2025, 441: 117992.
 49. Tong C, Sun ZL, Zhao QL, et al. A hybrid algorithm for reliability analysis combining Kriging and subset simulation importance sampling, *Journal of Mechanical Science and Technology*, 2015, 29(8): 3183-3193. <https://doi.org/10.1007/s12206-015-0717-6>
 50. Echard B, Gayton N, Lemaire M, et al. A combined importance sampling and Kriging reliability method for small failure probabilities with time-demanding numerical models, *Reliability Engineering and System Safety*, 2013, 111: 232-240. <https://doi.org/10.1016/j.ress.2012.10.008>
 51. Wang J, Sun ZL, Cao RN, et al. An efficient and robust adaptive Kriging for structural reliability analysis, *Structural and Multidisciplinary Optimization*, 2020, 62(6): 3189-3204. <https://doi.org/10.1007/s00158-020-02666-5>
 52. Yang XF, Liu YS, Fang XY, et al. Estimation of low failure probability based on active learning Kriging model with a concentric ring approaching strategy, *Structural and Multidisciplinary Optimization*, 2018, 58: 1175-1186. <https://doi.org/10.1007/s00158-018-1960-0>
 53. Yun WY, Lu ZZ, Jiang X, et al. AK-ARBIS: An improved AK-MCS based on the adaptive radial-based importance sampling for small failure probability, *Structural Safety*, 2020, 82: 101891.
 54. Zhang XF, Wang L, Sørensen JD. AKOIS: An adaptive Kriging oriented importance sampling method for structural system reliability analysis, *Structural Safety*, 2020, 82: 101876.
 55. Zhang XF, Wang L, Sorensen JD. REIF: A novel active-learning function toward adaptive Kriging surrogate models for structural reliability analysis, *Reliability Engineering and System Safety*, 2019, 185: 440-454. <https://doi.org/10.1016/j.ress.2019.01.014>
 56. Tabandeh A, Jia GF, Gardoni P. A review and assessment of importance sampling methods for reliability analysis, *Structural Safety*, 2022, 97: 102216.
 57. Zhang H, Song LK, Bai GC. Active Kriging-based adaptive importance sampling for reliability and sensitivity analyses of stator blade regulator, *Computer Modeling in Engineering & Sciences*, 2023, 134(3): 1871-1897. <https://doi.org/10.32604/cmescs.2022.021880>
 58. Deng K, Song LK, Bai GC, Li XQ. Improved Kriging-based hierarchical collaborative approach for multi-failure dependent reliability assessment, *International Journal of Fatigue*, 2022, 160: 106842.
 59. Li XQ, Song LK, Choy YS, Bai GC. Multivariate ensembles-based hierarchical linkage strategy for system reliability evaluation of

aeroengine cooling blades, *Aerospace Science and Technology*, 2023, 138: 108325.

60. Li XQ, Song LK, Bai GC. Vectorial surrogate modeling approach for multi-failure correlated probabilistic evaluation of turbine rotor, *Engineering with Computers*, 2023, 39(3): 1885-1904. <https://doi.org/10.1007/s00366-021-01594-2>
61. Song LK, Bai GC, Li XQ. A novel metamodeling approach for probabilistic LCF estimation of turbine disk, *Engineering Failure Analysis*, 2021, 120: 105074.
62. Gao HF, Wang YH, Li Y, Zio E. Distributed-collaborative surrogate modeling approach for creep-fatigue reliability assessment of turbine blades considering multi-source uncertainty, *Reliability Engineering & System Safety*, 2024, 250: 110316.
63. Li XQ, Song LK, Bai GC. Failure correlation evaluation for complex structural systems with cascaded synchronous regression, *Engineering Failure Analysis*, 2022, 141: 106687.
64. Bichon BJ, Eldred MS, Swiler LP. Efficient global reliability analysis for nonlinear implicit performance functions, *AIAA Journal*, 2012, 46(10): 2459-2468. <https://doi.org/10.2514/1.34321>
65. Yun WY, Lu ZZ, Jiang X. An efficient reliability analysis method combining adaptive Kriging and modified importance sampling for small failure probability, *Structural and Multidisciplinary Optimization*, 2018, 58: 1383-1393. <https://doi.org/10.1007/s00158-018-1975-6>
66. Wang Z, Shafieezadeh A. REAK: reliability analysis through error rate-based adaptive Kriging, *Reliability Engineering & System Safety*, 2019, 182: 33-45. <https://doi.org/10.1016/j.res.2018.10.004>
67. Yin M, Wang J, Sun Z. An innovative DoE strategy of the kriging model for structural reliability analysis, *Structural and Multidisciplinary Optimization*, 2019, 60(6): 2493-2509. <https://doi.org/10.1007/s00158-019-02337-0>

Appendix

Table A. Samples used for average angle

	x_{11}	x_{12}	x_{13}	x_{14}	x_{15}	x_{16}	x_{17}	x_{18}	x_{19}	x_{20}	α_{ave}
Initial	-79.522	134.974	50.011	50.017	80.017	50.02	199.988	99.984	114.929	40.009	35.548
samples	-79.827	135.018	49.997	49.976	79.968	49.996	199.997	99.982	114.967	39.983	35.713
	-80.2	135.074	50.009	49.999	80.035	50.031	199.962	100.022	115.012	40.042	36.184
	-79.303	135.025	49.997	50.011	80.051	50.013	199.976	100.017	115.052	40.01	35.145
	-79.86	135.003	50	50.003	79.986	49.987	199.952	100.004	115.02	39.993	35.786
	-79.925	135.011	50.012	50.008	79.998	49.994	199.991	99.991	115.008	40.01	35.921
	-80.275	134.995	50.026	49.99	80.014	49.992	199.97	99.977	114.985	39.998	36.561
	-80.383	134.946	50.01	49.991	80.039	50.005	199.983	100	115.003	40.023	37.019
	-80.595	135.055	50.029	49.995	80.015	50.015	200.002	100.041	115.028	39.991	36.865
	-80.165	135.109	49.96	49.974	80.009	49.99	199.966	100.014	114.993	39.974	35.719
	-80.354	134.956	49.992	50.022	79.982	50.011	200.01	100.006	115.047	40.005	36.721
	-79.802	135.193	50.004	49.993	79.991	50.033	200.019	100.025	114.967	40.031	35.042
	-80.095	134.976	49.984	50.008	80.022	50.021	199.972	100.023	114.991	39.97	36.305
	-79.59	134.972	49.973	49.971	80.046	50.018	200.037	99.955	114.998	39.989	35.775
	-79.603	134.931	50.015	49.964	80.018	49.978	199.946	100.003	114.94	40.021	35.944
	-79.977	134.941	50.014	49.99	79.965	49.985	199.997	99.987	115.018	39.956	36.286
	-80.078	134.926	50.006	49.988	80.011	50.005	199.951	99.95	115	40.012	36.567
	-79.695	135.021	50.008	50.016	79.996	49.997	200	99.963	115.002	40.015	35.513
	-80.453	135.133	49.983	50.006	79.989	49.968	199.959	99.992	115.021	40.003	35.896
	-79.789	135.032	49.991	50.005	79.992	49.971	199.989	100.032	115.032	39.98	35.55
	-80.213	135.067	49.999	49.941	79.97	50.023	199.981	99.995	115.024	39.998	36.227
	-80.158	135.106	49.986	49.968	79.985	49.983	199.968	100.008	114.987	40.001	35.77
	-80.228	134.808	50.007	49.998	79.97	50.061	199.922	99.977	114.997	40.018	37.36
	-79.847	134.98	50.038	49.984	79.983	49.956	200.025	99.944	115.009	40.012	36.007
	-80.293	135.02	49.992	50.018	80.003	50.009	200.055	100.003	114.965	39.986	36.007
	-80.383	135.043	50.016	50.02	80.005	49.997	200.058	99.974	114.971	40.036	36.426
	-79.854	134.902	49.977	49.977	79.993	49.983	199.994	100.042	114.989	39.997	36.318
	-80.177	134.916	50.024	50.013	79.996	50.008	200.008	100.077	114.999	39.979	36.828
	-79.907	135.058	49.98	50.021	80	49.981	199.995	99.989	115.042	39.984	35.52
	-80.112	134.985	50.003	50.001	80.013	50.019	200.011	100.046	115.023	40.016	36.44
	-79.934	135.034	49.989	50.03	80.042	50	199.974	100.036	114.988	40.003	35.784

-80.801	134.921	50.012	50.015	80.023	49.967	199.929	99.96	114.983	40.018	37.472	
-79.888	134.871	50.001	49.998	79.986	49.95	200.009	99.999	115.04	39.999	36.447	
-79.564	135.052	49.999	50.014	80.019	49.99	199.965	100.007	115.059	40.061	35.277	
-79.733	135.087	50.05	49.997	79.988	50.025	199.937	100.02	115.004	39.959	35.46	
-79.75	135.159	49.987	49.981	79.956	50.004	200.065	100.029	114.987	39.985	35.012	
-80.06	134.874	49.999	50.002	79.929	49.999	200.005	100.027	114.961	39.995	36.625	
-79.964	134.895	50.041	49.994	79.96	50.015	200.02	100.031	115.029	40	36.703	
-79.942	134.881	49.976	49.982	79.99	49.973	200.041	99.993	115.007	40.029	36.517	
-80.02	134.99	50.013	50.032	79.977	50.028	199.943	100.012	115.034	40.004	36.102	
-80.302	134.949	49.976	49.999	79.973	49.977	200.023	99.929	114.973	39.994	36.518	
-80.119	135.1	50.022	50.047	80.001	49.999	200.024	99.966	115.006	39.999	35.692	
-80.049	134.89	50.006	49.986	79.975	49.988	200.013	100.051	114.981	40.014	36.706	
-80.195	134.847	50.017	50.006	79.977	50.002	200.017	99.981	115.036	39.981	37.096	
-79.779	135.006	49.996	50.026	80.02	49.961	199.989	100.012	114.985	40.009	35.616	
-79.396	135.083	50.004	50.041	80.027	50.029	200.029	100.052	114.996	39.964	34.933	
-80.511	134.939	50.027	50.001	80.056	50.012	199.979	99.979	114.993	39.995	37.27	
-80.01	134.908	49.95	49.973	80.008	50.043	199.981	99.972	115.031	39.978	36.535	
-80.516	134.982	49.967	50.012	80.001	50.027	200.031	99.986	115.014	39.981	36.806	
-79.641	134.86	50.009	49.956	79.979	49.998	200.05	100.016	114.972	40.006	36.411	
-79.617	134.994	49.987	49.987	79.994	49.977	199.999	99.997	114.982	39.972	35.503	
-80.574	135.065	49.995	50	79.997	49.963	199.992	99.97	114.969	39.976	36.409	
-79.492	135.009	49.969	50.024	79.959	49.998	200.022	99.958	115.016	39.968	35.091	
-80.413	134.813	49.982	50.023	79.987	50.004	200.036	99.99	115.009	39.947	37.411	
-79.957	134.954	49.994	49.992	80.024	50.024	200.034	99.996	114.951	39.992	36.334	
-79.713	134.968	49.985	50.015	79.98	49.975	200.018	99.985	114.944	40.025	35.64	
-79.983	135.18	49.983	49.984	80.014	50.017	199.985	99.994	114.998	39.991	35.259	
-79.417	135.072	49.994	50.007	80.031	50.001	200.027	99.97	115.019	39.99	34.992	
-79.153	134.989	49.981	50.034	80.032	49.982	200.007	100.022	115.005	39.975	34.871	
-80	135.092	50.025	49.996	80.024	50.017	200.048	99.939	114.956	40.033	35.802	
-80.662	134.911	49.979	49.985	79.949	50.006	199.957	100.005	114.954	39.989	37.271	
-80.134	134.963	50.033	49.979	79.981	49.993	200.016	100.026	115.026	40.026	36.628	
-80.326	135.113	49.995	50.01	80.03	50.037	200.044	99.979	114.995	40.007	36.105	
-80.252	135.121	49.972	50.019	80.008	50.014	199.993	99.998	114.99	39.986	35.734	
-80.444	135.046	49.988	50.037	79.999	49.995	199.986	100.01	115.038	40.022	36.346	
-80.031	135.029	50.02	49.995	80.011	50.007	199.972	99.983	114.978	40.019	36.069	
-79.463	134.952	50.022	49.996	80.037	50.002	200.004	100	115.004	39.994	35.73	
-80.24	135.049	50.001	49.976	80.004	50.003	200.005	100.013	115.013	40.028	36.314	
-80.07	134.936	50.005	50.027	79.972	50.01	200.014	99.975	115.025	40.04	36.409	
-79.687	135.037	50.015	49.991	79.995	49.985	199.975	100.035	114.975	39.996	35.511	
Sequential samples	-79.665	135.016	49.971	49.98	79.994	49.98	200.013	100.038	115.01	39.987	35.509
	-79.882	135.079	49.99	50.04	80.028	50.008	199.987	100.01	115.073	40.008	35.518
	-79.737	134.96	49.963	50.012	80.01	50.041	200	100.001	114.96	40.007	35.839
	-79.772	135.039	49.993	50.009	80.017	49.989	199.98	99.968	115.014	40.015	35.523
	-80.144	135.062	50.02	49.966	80.003	49.974	200.003	100.017	114.994	39.988	36.118
	-79.898	134.927	50.018	50.004	79.984	49.992	200.081	99.964	114.977	40.013	36.322
	-80.086	135.001	50.035	50.004	80.002	49.986	200.072	100.061	114.976	40.021	36.364
	-80.342	135.138	50.002	49.962	80.006	49.989	200.039	100.02	115.016	40.002	36.076
	-79.821	134.998	49.954	49.988	79.963	50.012	200.031	100.009	115.05	40.002	35.756
	-80.039	134.967	50.032	49.982	80.006	49.994	199.963	99.988	114.98	39.969	36.383
	-79.889	135.145	49.996	50.011	80.001	49.997	200.006	100.01	114.987	39.992	35.211
	-79.529	135.07	49.99	50.006	80.001	49.992	200.033	99.994	115.023	40.004	35.096
	-79.806	135.148	50.012	50.008	79.984	49.989	200.005	100.002	114.987	39.981	35.084
	-79.797	135.15	49.997	50.017	79.995	50.016	200.011	100.036	114.99	39.998	35.107
	-79.416	135.132	50.004	50.004	79.985	49.991	199.992	100.03	114.983	40.008	34.663
	-79.391	135.152	50.009	50.005	79.985	50	200.037	99.996	114.984	39.991	34.574
	-79.279	135.127	49.985	50.013	80.005	49.986	199.986	100.005	115.033	40.011	34.466
	-79.427	135.152	49.999	49.979	80.024	49.979	199.975	100.022	115.003	40.023	34.698

-78.992	135.106	49.999	49.986	80.012	50	200.028	99.997	115.024	39.992	34.359
-78.994	135.054	50	50.015	80.017	50.008	199.949	100.005	115.022	39.98	34.482
-79.41	135.177	49.972	49.98	79.994	49.992	199.976	99.972	115.057	40.009	34.45
-79.446	135.189	49.977	50.004	79.969	50.025	199.931	100.012	114.99	40.02	34.372
-79.95	135.301	50.013	50.025	80.011	50.029	199.958	99.983	115.003	40.013	34.654
-79.293	135.145	50.012	50.021	79.997	49.94	199.987	99.979	115.054	39.997	34.343
-78.764	134.874	49.972	50.012	79.997	50.002	200.026	99.995	114.969	40.037	34.898
-79.403	135.178	49.989	50.066	79.987	49.957	199.968	99.992	115.034	40.01	34.153
-79.317	135.218	49.997	50.011	79.981	50.021	200.01	99.984	115.1	40.028	34.242
-78.685	135.088	49.991	49.944	79.995	49.984	200.035	99.959	115.03	40.016	34.074
-78.657	135.225	50.016	49.978	80	50.01	199.949	99.97	114.959	40.014	34.074
-78.919	135.032	50.018	50.056	80.026	49.936	200.002	100.058	115.011	40.017	34.37
-78.437	135.086	50.041	49.965	80	50.015	199.965	99.97	115.007	39.96	33.846
-78.182	135.058	49.982	50.029	80.001	50.006	200.042	99.942	114.998	40.004	33.331
-78.325	134.861	49.983	49.932	79.973	49.997	199.979	99.984	115.007	40	34.565
-78.912	135.063	50.006	50.058	79.908	49.953	200.024	100.042	114.974	40.032	34.005
-78.664	135.153	49.999	50.02	79.966	49.905	200.055	99.997	115.024	39.986	33.396
-78.425	135.094	49.967	50.004	79.997	50.055	200.071	100.077	115.036	40.037	33.752
-79.077	135.161	49.912	50.044	80.09	50.014	199.975	99.984	115.055	39.989	33.955
-79.304	135.365	49.935	50.066	80.023	49.969	199.964	99.997	115.077	39.986	33.188
-77.897	135.088	50.022	50.02	80.011	49.998	200.056	100.004	114.972	39.931	32.991
-78.398	135.267	50.04	50.033	80.021	50.043	199.897	99.96	115.054	39.972	32.919
-80.231	135.323	49.998	49.919	79.984	49.975	199.935	100.054	115.14	40.022	35.165
-78.21	135.279	49.957	50.045	80.024	50.037	200.058	99.908	114.987	40.024	32.42
-78.345	135.331	49.961	50.011	79.921	49.966	199.967	100.076	115.068	39.99	32.266
-77.956	135.318	50.057	50.021	80.047	49.978	200.048	99.983	115.055	39.965	32.274
-77.642	135.165	49.953	50.004	80.049	49.949	199.91	100.034	114.998	40.006	32.19

Table B. Samples used for maximum minimum angle error

	x_{21}	x_{22}	x_{23}	x_{24}	x_{25}	x_{26}	x_{27}	x_{28}	α_{err}
Initial samples	99.999	114.985	200.035	100.046	49.958	79.993	50.029	50.012	0.102
	99.995	115.061	199.963	100.061	50.003	79.995	49.99	49.988	0.199
	99.977	115.03	200.024	100.049	50.004	79.977	50.016	50.015	0.094
	100.016	114.989	200.013	99.987	50.003	80.014	49.968	49.97	0.056
	99.974	115.009	200.039	99.979	49.999	80.001	49.996	49.991	0.077
	99.979	114.975	199.985	99.999	49.981	80.014	50.031	49.979	0.089
	100.018	114.978	200.051	99.991	49.975	80.016	49.994	50.048	0.095
	99.971	115.04	200.03	100.027	50.002	79.995	50.013	50.015	0.11
	99.97	114.984	199.989	100.017	50.044	80.023	50.014	50.015	0.149
	99.934	115.074	200.041	100	49.942	80.036	50.021	50.04	0.192
	99.95	115.001	200.002	100.031	49.992	80.004	50.017	50.003	0.153
	99.98	115.038	199.99	100.003	49.953	79.986	49.99	50.026	0.068
	100.019	115.018	200.015	100.017	50	79.985	49.982	49.982	0.053
	99.956	115.033	199.973	100.032	49.988	80.054	50.025	50.035	0.238
	100.016	114.953	200.012	99.998	49.996	79.98	50.034	49.998	0.181
	99.986	114.994	200.018	99.952	50.025	79.976	49.996	49.995	0.086
	100.008	115.024	200.038	100.012	50.001	79.96	49.996	50.001	0.053
	100.037	115.027	199.955	100.044	50.006	80.018	50.012	49.985	0.132
	100.027	115.031	199.967	99.99	50.034	80.033	49.999	50.043	0.177
	99.972	114.998	199.968	99.993	50.023	80.004	50.027	50.001	0.089
	99.975	115.043	199.974	100.029	50.005	79.962	50.017	49.982	0.108
	100.01	115.006	199.993	99.98	50.02	80.013	49.957	49.996	0.072
	100.039	114.987	199.992	99.964	49.995	80.043	49.986	49.965	0.117
	100.001	114.98	199.997	100.001	50.01	80.01	49.987	50.023	0.043
	100.023	114.982	200.005	100.047	50.031	80.026	50.008	50.016	0.105
	99.997	114.944	199.987	100.013	50.009	80.003	49.978	50	0.018
	100.005	115	199.994	99.979	49.993	79.994	49.986	50.017	0.017

	100.009	115.011	200.027	100.01	50.011	80.005	49.993	50.02	0.049
	100.002	114.977	200.015	100.016	50.02	80.012	50.018	49.979	0.034
	99.999	114.992	199.979	99.991	50.039	79.972	49.963	50.024	0.098
	99.981	115.023	200.077	100.039	50.024	79.994	49.999	49.957	0.062
	99.971	115.011	199.969	100.03	50.012	79.995	50.007	49.971	0.113
	99.996	114.983	200.067	100.014	49.986	80.01	49.988	49.984	0.091
	99.99	115.028	200.006	100.006	49.988	80.02	49.977	50.031	0.119
	100.006	114.943	199.982	99.99	49.982	80.006	50.008	50.014	0.103
	99.987	115.016	199.979	100.013	50.025	80.007	50.007	49.954	0.072
	99.991	115.014	199.976	100.007	49.973	79.923	50.05	49.996	0.118
	100.047	114.981	200.016	99.95	50.014	79.971	49.952	49.991	0.161
	99.996	115.053	200.049	100.003	49.973	79.999	49.99	49.981	0.018
	99.932	115.026	200.02	99.996	50.011	80.022	50.02	50.037	0.216
	99.949	115.036	199.99	100.053	49.985	80.009	49.973	49.994	0.221
	99.988	114.995	199.985	99.944	50.018	79.978	50.023	49.985	0.075
	99.979	115.022	200.026	99.976	50.003	80.019	49.992	50.019	0.082
	99.993	114.968	200.032	99.982	49.977	79.973	50.057	50.02	0.203
	99.989	114.972	199.982	99.989	50.004	79.996	49.983	50.018	0.031
	99.977	114.982	200.007	99.999	49.997	79.969	50	49.986	0.084
	99.961	115.004	199.971	99.986	50.002	79.961	49.979	50.029	0.118
	99.978	114.998	199.995	99.984	49.983	80.009	50.013	50.017	0.066
	99.986	114.983	200.009	100.015	49.994	79.945	50.047	50	0.12
	99.999	115.029	200.002	99.987	49.99	80.007	49.998	49.949	0.027
	99.989	115.013	200.016	100.027	49.986	80.002	49.993	49.989	0.048
	99.985	114.955	200.003	99.997	49.995	80.006	50.021	49.995	0.089
	99.976	114.969	199.989	100.012	49.987	80.016	49.974	49.993	0.065
	99.982	114.954	200.054	100.068	49.993	80.035	49.966	50.002	0.055
	100.01	115.027	200.005	99.962	49.978	80.029	49.964	50.011	0.037
	100.034	115.038	200.088	99.981	50.063	80.041	50.014	50.05	0.138
	99.997	114.981	199.964	100.041	49.985	80.001	49.985	50.001	0.058
	100.031	115.005	199.96	100.001	49.979	79.956	50.043	50.023	0.111
	100.031	115	200.036	99.997	50.028	79.975	50.016	49.99	0.112
	99.99	114.97	200.046	100.039	49.981	79.987	49.991	49.998	0.08
	99.969	115.039	199.964	100.022	50.014	79.993	50.002	49.992	0.172
	99.973	114.995	200.001	99.978	50.005	79.966	49.987	50.011	0.065
	100.001	115.011	200.053	100.024	49.968	79.952	50.013	49.993	0.144
	99.994	115.05	199.997	100.037	50.018	80.012	49.977	50.01	0.202
	100.017	114.984	199.951	99.953	50.026	79.979	50.012	50.005	0.059
	99.978	115.019	200.047	99.996	49.989	80	50.007	49.973	0.079
	99.964	115.029	199.997	100.008	50.02	80.015	50.024	50.008	0.155
	100.015	114.99	199.934	100.001	50.019	80.037	50.003	49.984	0.091
	99.983	115.02	199.972	99.985	50.05	79.968	49.995	50.018	0.134
	100.013	114.999	200.042	99.983	50.04	80.012	50.01	50.024	0.046
Sequential samples	100.028	115.017	200.011	99.997	49.998	80.011	50.012	50.019	0.07
	100.019	115.022	200.033	100.036	50.037	80.005	50	49.978	0.077
	99.981	115.043	200.007	99.995	50.021	80.029	50.001	50.013	0.161
	100.071	115.044	200.044	100.015	49.978	80.025	50.001	49.944	0.201
	99.963	114.988	200.024	99.958	49.999	80.007	50.037	50.065	0.101
	100.015	115.048	200.062	100.021	49.974	80.004	49.951	50.003	0.061
	100.024	114.997	199.959	100.022	49.998	79.989	49.999	50.009	0.081
	99.992	114.967	199.971	99.971	49.991	79.999	50.026	49.975	0.108
	100.013	114.937	200.022	99.976	49.961	80.044	50.043	50.023	0.209
	100.032	114.931	199.993	99.998	49.984	80.019	49.97	50.011	0.121
	100.025	115.008	199.955	100.056	49.963	80.034	49.997	50.043	0.122
	100.007	115.007	199.991	100.017	50.012	79.997	50.019	49.977	0.02
	100.038	114.974	200.037	100.024	50.006	79.994	50.006	49.997	0.138
	99.959	115.001	200.01	100.015	50.007	79.998	49.998	49.999	0.117

100.025	114.993	199.97	100.028	49.971	80.005	50.041	49.99	0.091
99.996	115.009	200.029	99.965	50.019	80.013	49.996	50.001	0.018
99.961	114.997	199.97	99.973	49.996	80.015	50.014	49.997	0.103
100.041	115.008	199.939	99.989	49.97	79.969	50.039	50.01	0.127
100.002	115.022	199.984	100.009	49.992	80	50.002	50.027	0.087
99.967	115.014	199.976	100.007	50.032	80.014	50.002	49.995	0.164
99.965	114.947	199.957	100.006	49.995	79.996	49.972	49.978	0.091
100.045	114.958	200.057	100.04	49.967	79.988	50.028	50.008	0.245
100.011	115.041	200.032	99.974	50.028	80.027	49.992	50.005	0.079
99.958	115.027	199.943	100.033	50.009	79.954	50.021	49.997	0.159
100.027	115.066	199.965	99.977	49.979	79.997	49.985	49.983	0.093
99.975	114.989	199.953	100.011	50.013	80.032	49.992	49.977	0.126
100.011	114.976	200.004	99.981	50.006	80.027	50.003	50.021	0.033
100.05	115.003	200.013	100.03	49.997	80.012	49.978	49.964	0.135
99.957	115.005	199.978	99.94	50.03	79.986	49.997	50.01	0.119
100.026	114.97	199.996	100.01	50.008	79.983	49.989	49.987	0.092
99.98	114.999	199.986	100.028	49.992	80.03	50.01	49.975	0.07
100.01	114.964	200.008	99.968	49.984	80.02	50.005	50.007	0.118
99.97	115.024	199.919	100.007	50	79.968	50.018	49.968	0.113
100.021	114.999	200.027	99.936	50.009	79.988	49.975	50.009	0.097
99.951	115.035	199.967	100.042	50.022	79.986	49.997	50.007	0.247
99.984	115.056	200.008	100.01	50.016	80.011	50.019	50.007	0.134
100.045	115.03	200.055	99.971	49.98	79.974	49.994	49.991	0.192
99.993	115.002	199.986	99.968	50.01	80.015	50.008	49.995	0.022
99.988	115.035	199.993	99.965	50.007	80.019	49.991	50.021	0.103
99.998	115.003	200.021	100.019	49.987	79.949	50.006	49.998	0.077
100.024	114.997	200.023	100.018	49.986	79.948	50.007	49.986	0.15
100.006	115.033	200.022	99.972	50.011	80.017	49.968	49.987	0.05
99.992	114.973	200	99.993	49.98	79.975	49.981	50.026	0.051
100.066	114.973	200.023	100.016	50.009	79.998	50.031	50.032	0.19
100.017	114.995	200.02	99.962	49.993	80	50.027	50.012	0.125
100.005	114.987	200.083	99.963	50.005	80.04	49.994	49.994	0.109
100.022	115.013	200.005	100.005	49.994	79.967	50.023	50.002	0.086
99.96	115.015	200.038	100.052	49.983	79.963	50.011	50.004	0.104
99.994	114.996	199.944	100.008	50.008	79.989	49.991	49.992	0.073
99.967	115.098	200.017	100.026	49.987	79.995	49.995	50.016	0.21
100.052	115.021	199.98	99.942	49.948	80.022	49.967	50.008	0.147
99.988	115.002	200.018	100.023	49.997	79.982	49.993	50.014	0.036
100.005	115.01	199.998	99.99	49.991	80.038	50.008	50.036	0.059
100.02	114.988	199.935	100.003	49.998	79.991	50.005	50.006	0.073
100.023	114.963	200.033	99.966	49.974	79.992	49.994	49.999	0.211
100.004	115.007	199.93	99.985	49.999	80.017	50.001	49.997	0.078
100	114.989	199.986	100.02	49.998	79.985	49.995	50.002	0.025
99.991	114.96	200.014	99.983	50.036	80.049	49.969	50.006	0.073
99.995	115.02	199.981	100.004	49.969	80.024	50.016	49.994	0.035
100.016	114.986	199.998	100.026	50.049	79.979	49.987	49.986	0.062
99.987	114.986	199.995	99.977	50.007	80.024	50.033	49.983	0.061
99.99	114.971	200.01	100.002	49.989	79.992	49.98	49.969	0.081
100.035	115.037	199.966	99.986	50.012	80.021	49.983	49.994	0.124
100.032	115.015	199.988	99.996	49.977	79.959	49.999	50.003	0.123
99.963	115.007	200	99.947	49.99	80.004	49.977	50.018	0.095
99.976	115.017	200.001	99.981	50.002	80.032	50.028	50.014	0.085
100.057	115.017	200.011	99.98	49.995	79.983	49.984	49.989	0.161
99.984	115.003	200.004	100.01	50.022	80.052	49.965	50.001	0.166
100	114.956	199.958	100.019	49.976	80.026	49.983	49.98	0.022
99.988	114.977	199.99	100.023	49.994	79.984	49.985	49.999	0.036
99.954	115.052	200.007	99.992	49.97	79.97	49.984	49.978	0.118

100.048	114.967	199.996	99.998	49.959	80.009	50.003	49.962	0.233
100.002	114.961	200.019	99.994	50.013	80.031	50.03	49.966	0.11
99.945	114.985	199.892	99.988	50.016	80.047	50.024	50.025	0.248
99.969	114.99	199.949	99.978	50.021	79.984	50.037	49.973	0.084
99.981	115.032	200.009	99.969	50.014	80.06	50.005	49.996	0.114
100.022	115.012	200.013	99.931	50.007	80.018	50.019	49.987	0.116
100.028	114.994	199.987	99.987	50.035	79.998	50.015	49.962	0.095
100.011	115.01	199.982	100.034	50	79.992	50.032	49.967	0.032
99.943	114.965	199.979	100.057	50.01	79.99	50.023	50.022	0.165
100.021	114.99	200.036	100.05	49.988	79.972	49.989	49.991	0.091
99.984	114.996	199.954	100.044	49.965	80.022	50.009	50.009	0.09
100.043	114.979	199.962	99.96	49.964	79.975	50.004	49.974	0.225
99.998	115.019	199.95	99.975	50.001	80.039	50.006	50	0.093
100.009	114.971	200.05	99.973	50.025	80.008	49.998	50.006	0.095
100.033	114.951	199.984	100.005	49.979	79.971	50.035	49.976	0.242
99.947	114.976	200.065	100	50.011	80.003	49.988	49.988	0.148
99.94	114.978	200	99.984	49.991	79.941	50.004	50.013	0.177
99.986	114.966	199.968	100.011	49.982	79.988	50.02	49.985	0.071
99.974	115.046	199.98	100.063	50.017	79.964	49.971	50.016	0.233
100.004	114.959	200.029	99.97	50.015	80.01	49.976	49.992	0.078
100.03	115.058	200.029	99.961	50.015	80.028	50.01	50.002	0.088
99.924	115.025	199.962	99.948	49.996	79.987	50	49.968	0.195
100.019	114.979	199.999	99.97	49.972	79.978	50.015	49.974	0.207
100.003	115.047	199.976	99.975	50.024	80.046	49.98	50.027	0.2
99.994	114.948	199.94	100.088	49.983	79.99	49.979	50.011	0.085
99.973	114.963	200.072	100.002	50	80.002	50.011	50.013	0.112
99.966	115.025	200.019	100.037	49.972	80.001	49.989	49.972	0.094
100.06	114.961	199.992	100.002	49.996	79.982	50.022	49.999	0.22
100.056	115.016	199.977	99.999	50.013	80.023	50.012	49.99	0.14
100.017	115.009	199.988	100.018	50.008	79.997	49.99	50.031	0.086
100.001	115.008	199.975	100.036	49.989	79.993	49.961	49.989	0.079
100.014	114.996	199.991	99.984	50.042	79.991	49.98	50.03	0.082
99.997	114.985	200.001	99.995	50.031	80.025	49.998	49.981	0.036
100.034	115.019	199.983	100.025	50.018	79.965	50.011	49.989	0.095
100.04	114.993	199.983	99.992	50.001	80.021	49.975	50.029	0.128
100.039	115.006	200.003	100.033	49.994	80.002	49.931	50.004	0.129
100.012	114.994	200.043	99.91	50.002	79.988	50.009	50.005	0.187
100.014	115.033	199.925	99.974	49.975	79.99	50.004	49.971	0.042
100.092	115.013	200.028	99.991	49.957	79.985	50.025	49.98	0.338
100.006	115.001	199.974	100.009	50.002	80	50.018	50.039	0.06
100.003	114.991	199.974	99.994	50.006	79.982	50.015	49.988	0.046
100.007	114.975	200.009	100.013	50.027	79.98	49.988	50.005	0.042
99.983	114.982	199.961	99.959	49.966	80.003	49.981	50.008	0.054
99.953	114.993	200.045	99.988	50.033	79.981	50.009	50.034	0.114
100.029	115.014	200.021	99.992	49.985	80.033	49.986	49.993	0.079
99.993	115.003	199.947	99.993	50.027	80.016	50.001	50.004	0.122
100.013	115.012	200.025	100.02	50.015	80.065	49.959	49.984	0.119
100.02	114.965	200.031	100.035	49.988	79.976	49.976	50.028	0.077
100.028	115.021	200.035	100.006	49.983	79.999	49.991	49.96	0.116
100.042	114.98	199.945	99.967	50.016	80.008	50.005	50.022	0.108
100.008	114.949	200.003	100.014	49.991	79.979	49.993	50.006	0.103
99.983	115.005	200.059	100.004	50.029	79.983	49.971	49.982	0.052
99.995	115.004	200.017	100.021	50.004	79.981	50.003	50.033	0.044
100.012	114.94	200.041	100.005	50.017	79.996	49.973	50.003	0.098
100.003	114.987	200.012	99.956	49.999	79.974	49.982	49.996	0.102
100.008	114.992	199.994	99.956	49.99	79.991	50	50.012	0.075
100.054	114.915	200.026	99.985	50.022	80.008	50.002	49.958	0.276

100.036	114.991	200.015	100.025	50.004	79.958	49.955	49.981	0.11
99.968	114.974	199.999	99.954	49.98	80.006	49.984	50.019	0.097
